5 Water and Energy Balances at Soil-Plant-Atmosphere Interfaces

Steven R. Evett

5.1 INTRODUCTION

Energy fluxes at soil-atmosphere and plant-atmosphere interfaces can be summed to zero because the surfaces have no capacity for energy storage. The resulting energy balance equations may be written in terms of physical descriptions of these fluxes; and have been the basis for problem casting and solving in diverse fields of environmental and agricultural science such as estimation of evapotranspiration (ET) from plant canopies, estimation of evaporation from bare soil, rate of soil heating in spring (important for timing of seed germination), rate of residue decomposition (dependent on temperature and water content at the soil surface), and many others. The water balances at these surfaces are implicit in the energy balance equations. The soil water balance equation is different from, but linked to, the surface energy balances; a fact that has often been ignored in practical problem solving. In this chapter the energy balance will be discussed first, followed by the water balance in section 5.2.

Computer simulation has become an important tool for theoretical investigation of energy and water balances at the earth's surface, and for prediction of important results of the mechanisms involved. This chapter will focus more on the underlying principles of energy and water balance processes, and will mention computer models only briefly. More information on computer models that include surface energy and water balance components can be found in Anlauf et al. (1990), ASAE (1988), Campbell (1985), Hanks and Ritchie (1991), Peart and Curry (1998), Pereira et al. (1995), and Richter (1987) to mention only a few.

5.2 ENERGY BALANCE EQUATION

The surface energy balance is

$$0 = Rn + G + LE + H \qquad [5.1]$$

where Rn is net radiation; G is soil heat flux; LE is the latent heat flux (evaporation to the atmosphere) and is the product of the evaporative flux, E, and the latent heat of vaporization, L; and H is sensible heat flux (all terms taken as positive when flux is towards the surface, and in W m^{-2}). Each term may be expressed more completely as the sum of subterms that describe specific physical processes, some of which are shown in Fig. 5.1. Thus, net radiation includes the absorption and reflection of shortwave radiation (sunlight, Rsi and the reflected portion αRsi), as well as the emission and reception of longwave radiation (L↑ and L↓, respectively, Fig. 5.1). Soil heat flux involves not only diffusion of heat, G, as expressed by Fourier's law (see Chapter 9), but also convective heat flux, G_{Jw}, as water at temperature T flows at rate J_w into soil at another temperature T′. Both evaporation from the soil and from plants are examples of latent heat flux; but so also is dew formation, whether it wets the soil surface or plant canopy. Finally, sensible heat flux may occur between soil and atmosphere or between plant and atmosphere, and may be short-circuited between soil and

This chapter was prepared by a USDA employee as part of his official duties and cannot legally be copyrighted. The fact that the private publication in which the chapter appears is itself copyrighted doesn not affect the material of the U.S. Government, which can be reproduced by the public at will.

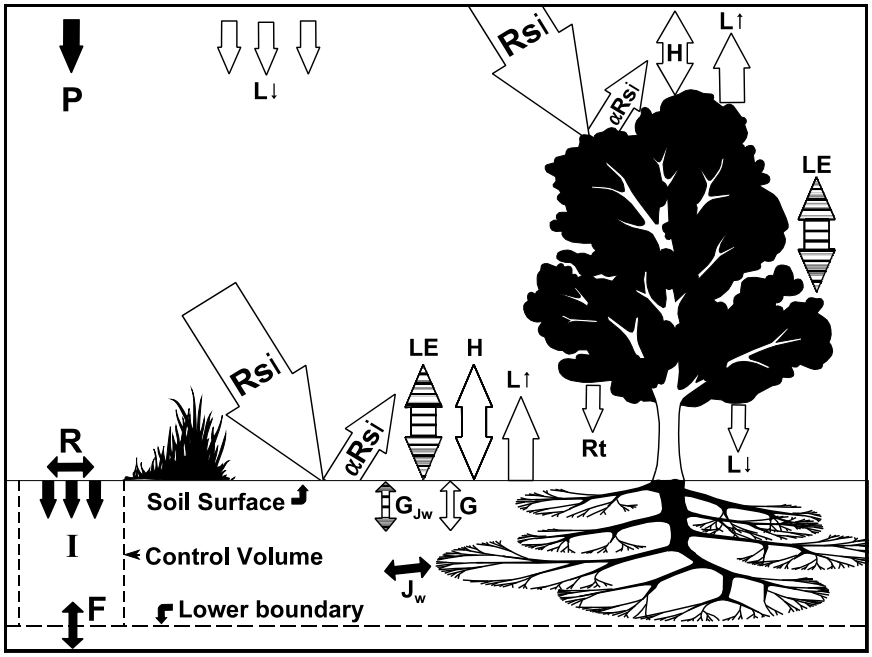

Fig. 5.1 Water and energy balance components. Water balance components are in black, energy balance components in white. The shared term LE is shaded. Water balance is discussed in section 5.3.

plant, for example when sensible heat flux from the soil warms the plant. In the next few paragraphs these fluxes and values they may assume will be illustrated with examples from some contrasting surfaces under variable weather conditions.

Values of these energy fluxes change diurnally (Figs. 5.2-5.4) and seasonally (Figs. 5.5 and 5.6). Regional advection is the large scale transport of energy in the atmosphere from place to place on the earth's surface. Regional advection events can change the energy balance greatly as illustrated with measurements taken over irrigated wheat at Bushland, TX (35°11′N Lat; 102°06′W Long) for the 48 h period beginning on day 119, 1992 (Fig. 5.2). Total Rsi was 26.1 and 26.7 MJ m^{-2} on days 119 and 120, respectively; close to the expected maximum clear sky value of 28.6 MJ m^{-2} for this latitude and time of year. However, on day 119 strong, dry, adiabatic southwesterly winds (mean 5 m s^{-1}, mean dew point 4.1 °C, mean T_{2m} 20.1 °C) caused H to be strongly positive, providing the extra energy needed to drive total LE to -32.8 MJ m^{-2}, even though both Rsi and Rn levels were reduced in the afternoon due to cloudiness. Total LE was much larger in absolute magnitude than Rsi and Rn totals. The next day the total LE was 39% smaller due to the absence of regional advection, even though total Rsi and Rn values were slightly higher. G values were near zero during this period of full canopy cover when leaf area index (LAI) was 7 (Leaf area index is defined as the single-sided surface area of leaves per unit land area). Note that net radiation was negative at night. This is indicative of strong radiational cooling of the surface, which radiates heat into the clear, low humidity nighttime skies common to this semi-arid location at 1170 m above mean sea level.

Over alfalfa in late summer, Rsi totals were lower (20.1 and 5.4 MJ m^{-2}, respectively, for days 254 and 255, 1997, Fig. 5.3). On the very clear day 254 peak Rsi was 798 W m^{-2}; and with regional advection occurring, LE flux was high. The 3 h period of negative H just after sunrise was due to the sun-warmed crop canopy being at higher temperature than the air. The arrival of a cool front bringing cloudy skies near midnight causes all fluxes to be much lower on day 255, with Rsi reaching only 220 W m^{-2}, and H hovering near zero for much of the day. The arrival of the cloud cover and moist air is signaled near midnight by the abrubt change from negative values of Rn and LE to near zero values. In the case of net radiation this is due

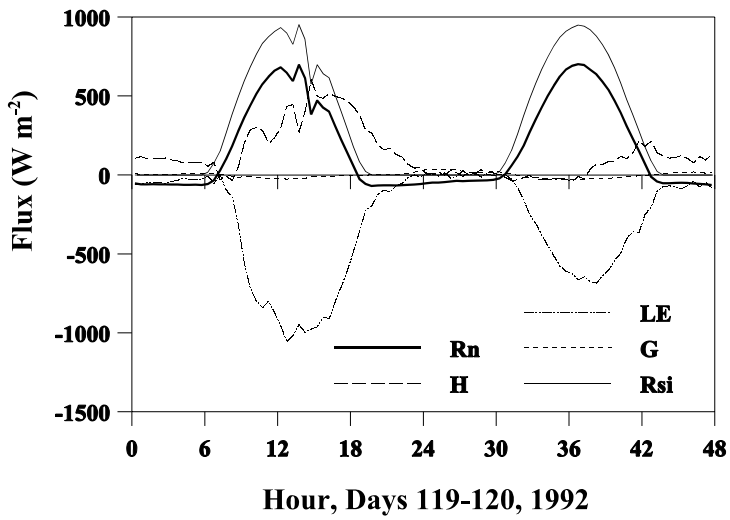

Fig. 5.2 Energy balance over irrigated winter wheat at Bushland, TX

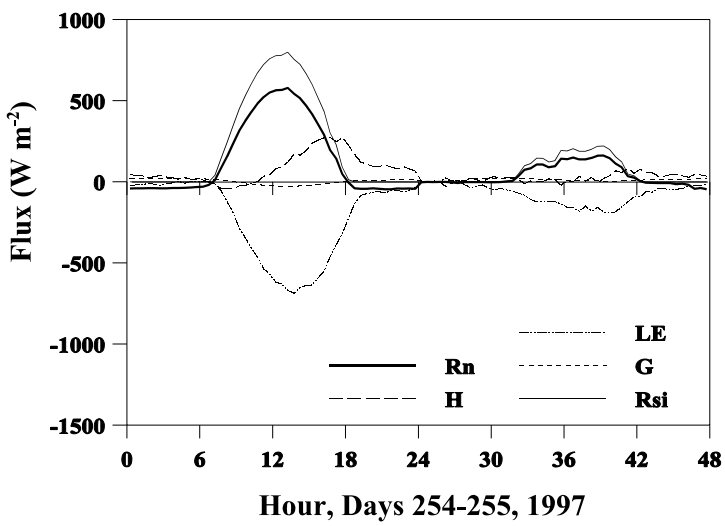

Fig. 5.3 Energy balance over irrigated alfalfa at Bushland, TX

to the increased longwave radiation from the clouds, which were warmer and had higher emissivity than the clear sky that preceded them. Latent heat flux nears zero because the strong vapor pressure gradient from moist crop and soil to dry air is reduced by the arrival of moist air. Note that after sunset, but before midnight, latent heat flux was strong, due to continuing strong sensible heat flux, even though net radiation was negative. Again, due to full crop cover (LAI = 3), G values are low, indicating that very little energy is penetrating the soil surface.

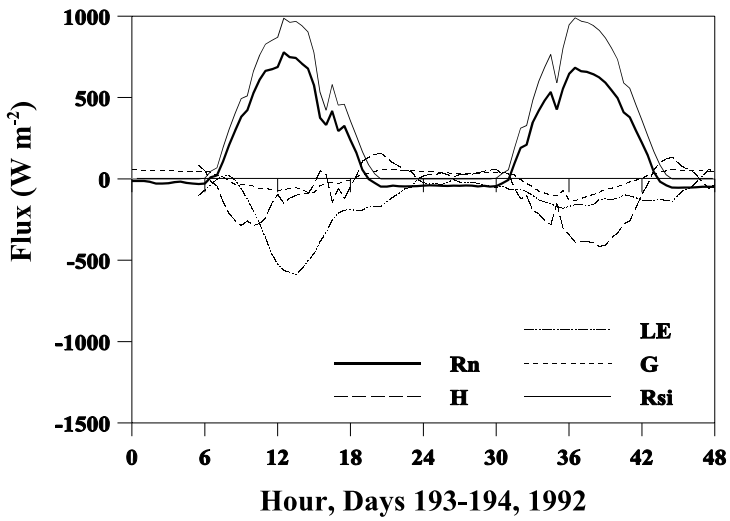

Fig. 5.4 Energy balance for bare Pullman clay loam soil after 35 mm of rain at Bushland, TX

For bare soil, G is often larger, becoming an important part of the energy balance (Fig. 5.4). After rain and irrigation totaling 35 mm over the previous two days, the soil was wet on day 193, 1992 at Bushland, TX. Latent heat flux totaled -14.4 MJ m^{-2} or 6 mm of evaporation; 77% of Rn. Sensible heat flux was negative for the first few hours after sunrise because the soil was warmer than the air, which had been cooled by a nighttime thunderstorm. Later in the day H and G both approached zero, and near sunset they became positive, supplying the energy consumed in evaporation that continued well into the night hours. Strong radiational cooling occurred on the nights of days 193 and 194 as indicated by negative values of Rn. Evaporation was probably energy-limited on day 193, becoming soil-limited on day 194. Latent heat flux on the second day was reduced to -7.4 MJ m^{-2}, and peak daytime values were not much larger than those for G. The drying soil became warmer and contributed heat to the atmosphere during almost all daylight hours.

Seasonal variations in daily total energy flux values occur due to changes of sun angle, of distance from the earth to sun (about 3% yearly variation), of seasonal weather, and of surface albedo as plant and residue cover changes (Figs. 5.5 and 5.6). A curve describing clear sky solar radiation at Bushland, Texas could be fit to high points of Rsi in Figs. 5.5 and 5.6. Net radiation was similar for alfalfa and bare soil except for a rainy period beginning about day 190 when the soil was wet and dark and Rn for the fallow field was markedly larger. The big differences were in LE and H. Latent heat flux from the alfalfa was large, reaching nearly -40 MJ m^{-2} (16 mm) on day 136 during a regional advection event that allowed LE to be larger than Rsi. Sensible heat flux was positive during much of the year. Soil heat flux was small during the growing season, becoming larger as the soil cooled during the fall and winter. For the bare soil, LE values were small during the first 150 days, the latter end of a drought. Sensible heat flux was negative during this period, and remained negative after rains began until day 203. Evaporative fluxes were fairly small, rarely reaching 6 mm d^{-1} even after rains began. In contrast to alfalfa, soil heat flux for bare soil was larger and more variable throughout the year.

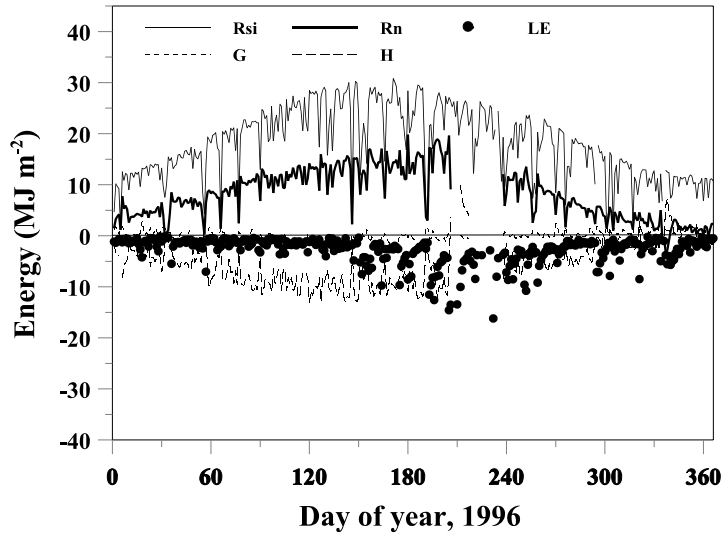

Fig. 5.5 Daily totals of energy balance terms for a fallow field (mostly bare Pullman clay loam) at Bushland, TX

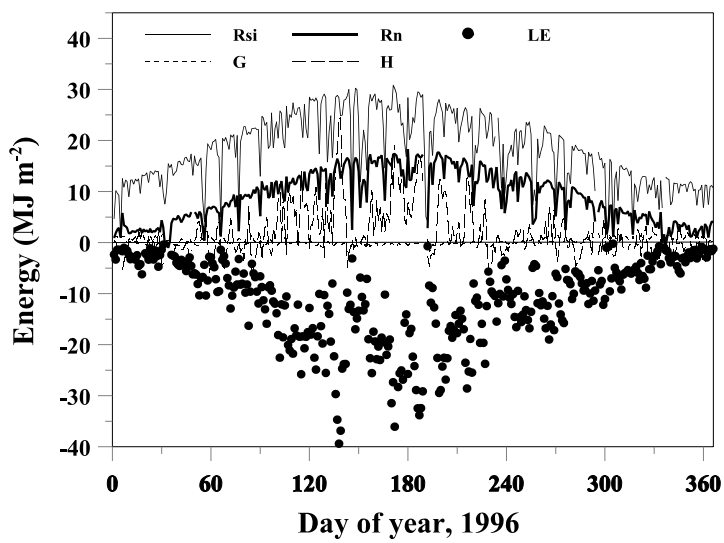

Fig. 5.6 Daily totals of energy balance terms for irrigated alfalfa at Bushland, TX

Methods of measurement and estimation of the energy fluxes are needed to characterize the energy balance. Examples of the instrumentation[1] needed to measure components and subcomponents of the energy balance are given in Table 5.1. These will be discussed in the following sections.

[1]*The mention of trade or manufacturer names is made for information only and does not imply an endorsement, recommendation, or exclusion by USDA-Agricultural Research Service.*

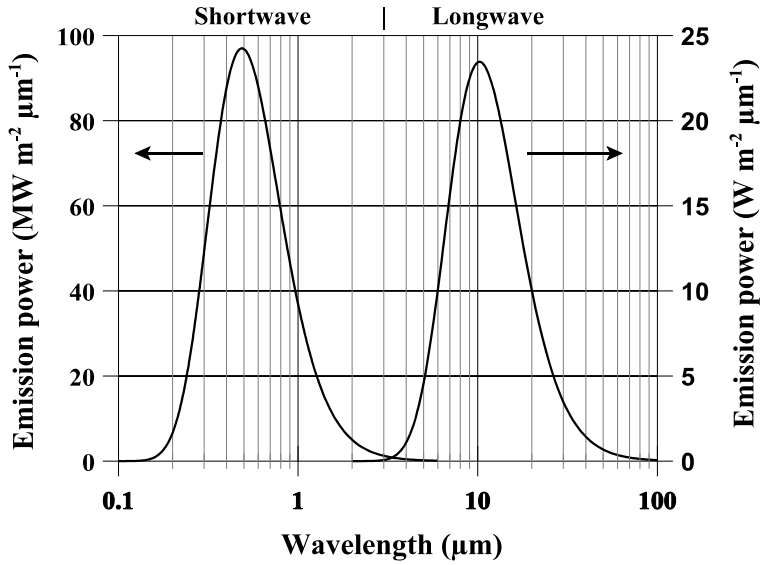

Fig. 5.7 Emission power spectra for ideal black bodies at 6000 K (left, shortwave range) and 285 K (right, long wave range)

5.2.1 Net Radiation

Net radiation is the sum of incoming and outgoing radiation

$$Rn = Rsi(1 - \alpha) - \epsilon\sigma T^4 + L\downarrow \qquad [5.2]$$

where Rsi is solar irradiance at the surface, α is the albedo or surface reflectance (0 to 1), ϵ is the surface emissivity (0 to 1), σ is the Stefan-Boltzmann constant (5.67×10^{-8} W m^{-2} K^{-4}), T is surface temperature (K), and L↓ is longwave irradiance from the sky. The sun radiates energy like a black body at about 6000 K while the earth radiates at about 285 K. The theoretical maximum emission power spectra for these two bodies overlap very little (Fig. 5.7), a fact that leads to description of radiation from the earth (including clouds and the atmosphere) as longwave, and radiation from the sun as shortwave. Note that the radiance of the earth is about 4 million times lower than that of the sun (Fig. 5.7). Net radiation may be measured by a net radiometer (Fig. 5.8) or its components may be measured separately using pyranometers to measure incoming and reflected short wave radiation, and pyrgeometers to measure incoming and outgoing long wave radiation (first four instruments in Table 5.1). Pyranometers and pyrgeometers are thermopile devices that are sensitive equally across the spectrum.

5.2.1.1 Outgoing Long Wave Radiation

The longwave radiance of the earth's surface, L↑, is given by the Stefan-Boltzmann law for radiance from a surface at temperature T and with emissivity ϵ.

$$L\uparrow = \epsilon\sigma T^4 \qquad [5.3]$$

An inverted pyrgeometer (Table 5.1) may be used to measure L↑ and, if accompanied by suitable surface temperature measurements, may allow estimation of surface emissivity, ϵ, by inversion of Equation [5.3]. Surface temperature is often measured by suitably placed and shielded thermocouples, or by infrared thermometer (IRT); though there are problems with either type of measurement (radiational heating of the thermocouples, and uncertainty of the emissivity needed for accurate IRT measurements).

Values of α and ϵ for soil and plant surfaces may be estimated from published values relating them to surface properties (see section 5.1.1.3 and Table 5.4). For soil, the dependence of α on water content is strong, but nearly linear, and amenable to estimation.

Table 5.1 Instruments and deployment information for bare soil radiation and energy balance experiments at Bushland, TX, 1992 (adapted from Howell et al., 1993). Parameters not shown in Fig. 5.1 will be presented later.

Parameter	Instrument	Manufacturer† (Model)	Elevation	Description
R_{si}	Pyranometer	Eppley (PSP)	1 m	Solar irradiance
αR_{si}	Pyranometer	Eppley (8-48)	1 m (I‡)	Reflected solar irradiance
L↓	Pyrgeometer	Eppley (PIR)	1 m	Incoming long wave radiation
L↑	Pyrgeometer	Eppley (PIR)	1 m (I)	Outgoing long wave radiation
R_n	Net Radiometer	REBS (Q*6)	1 m	Net radiation
T_s	Infrared Thermometer	Everest (4000; 60 º fov)	1 m nadir view angle	Soil surface temperature
T_a RH	thermistor foil capacitor	Rotronics (HT225R)	2 m	Air temperature & relative humidity
U_2	dc generator cups	R.M. Young (12102)	2 m	Wind speed
U_d	potentiometer vane	R.M. Young (12302)	2 m	Wind direction
T_t	Cu-Co thermocouple	Omega (304SS)	-10 mm -40 mm	Soil temperature (4)§
G_{50}	plates thermopile	REBS (TH-1)	-50 mm	Soil heat flux (4)
$\theta_{v\text{-}20}$ $\theta_{v\text{-}40}$	3-wire TDR probe	Dynamax TR-100/20 cm	-20 & -40 mm horizontal	Soil water content (2)
E_m	lever-scale load cell	Interface (SM-50)	Below lysimeter box	Lysimeter mass change

† Manufacturers and locations are: The Eppley Laboratory, Inc., Newport, RI; Radiation and Energy Balance Systems (REBS), Seatlle, WA; Everest Interscience, Inc., Fullerton, CA; Rotronic Instrument Corp., Huntington, NY; R.M. Young Co., Traverse City, RI; Omega Engineering, Inc., Stamford, CT; Dynamax, Inc., Houston, TX; Interface, Inc., Scottsdale, AZ.
‡ I designates instruments that were inverted and facing the ground.
§ Numbers in parentheses indicate replicate sensors.

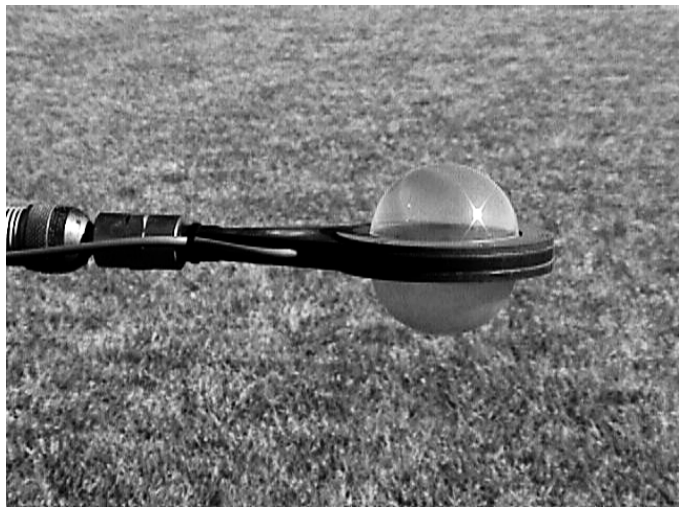

Fig. 5.8 REBS Q*7 net radiometer

5.2.1.2 Solar Irradiance

Solar irradiance, Rsi, includes both direct beam and diffuse shortwave radiation reaching the earth's surface; and is defined as the radiant energy reaching a horizontal plane at the earth's surface. It may be easily measured by pyranometer with calibration to international standards (Table 5.1) or by solar cells. Silicon photodetector solar radiation sensors such as the LI-COR model LI-200SA are sensitive in only part of the spectrum, but are calibrated to give accurate readings in most outdoor light conditions. Silicon sensors are much cheaper than thermopile pyranometers and have found widespread use in field weather stations. Measurement of both incident (Rsi) and reflected (Rsr) shortwave allows estimation of the albedo from

$$Rsi(1 - \alpha) = Rsi - Rsr \qquad [5.4]$$

This is done using upward and downward facing matched pyranometers (Table 5.1). Specially made albedometers are available for this purpose (e.g. Kipp & Zonen model CM-14) (Fig. 5.9).

The 'solar constant' is the flux density of solar radiation on a plane surface perpendicular to the direction of radiation and outside the earth's atmosphere. It is about 1370 W m^{-2}, with a variation of about ± 3.5%, being largest in January when the sun is closest to the earth, and smallest in July (Jones, 1992). Several satellite observation platforms have recorded the value of solar irradiance over nearly a 20 year span (Fig. 5.10) and clearly show the average solar cycle of 11 years. The six sets of data shown range over about 10 W m^{-2} or about 0.7% of the mean value. Thus, considering the 'solar constant' to be 1370 W m^{-2} will introduce no more than a 1% error in calculations.

Irradiance at the earth's surface is somewhat less, due to absorption and scattering in the atmosphere and due to sun angle effects; not often exceeding 1000 W m^{-2}. The further the sun is from the zenith the longer the transmission path through the atmosphere, and the more absorption and scattering occurs. Also, as sun angle above the horizon, β, decreases (it is highest at solar noon) the radiation density on a horizontal surface decreases according to Lambert's law

$$I = I_o \sin\beta \qquad [5.5]$$

where I_o is the flux density on a surface normal to the beam.

Sun angle (β) changes with time of day and year; and can be calculated from

$$\beta = \sin^{-1}[\sin(D)\sin(L) + \cos(D)\cos(L)\cos(H)] \qquad [5.6]$$

where L is latitude, D is solar declination, and H is solar time angle (all radians). Solar time angle is defined as

$$H = \frac{(T - T_{SN})2\pi}{24} \qquad [5.7]$$

where T is time (h), and T_{SN} is the time of solar noon. The time of solar noon varies with time of year and longitude according to (recall that 1° longitude = 4 min)

$$T_{SN} = 12 + \frac{4(Longitude - Local\ Meridian)}{60} - T_{EQ} \qquad [5.8]$$

where T_{EQ} is the 'equation of time' value (h), Longitude is in degrees, and the Local Meridian is the longitude (°) for which standard time is calculated for the time zone in question. In the U.S. the meridians for Eastern Standard Time (EST), Central Standard Time (CST), Mountain Standard Time (MST), and Pacific Standard Time (PST) are 75°, 90°, 105°, and 120°, respectively. Local or true solar time (T_{LS}) for any local standard time (T_{ST}) may be calculated with

$$T_{LS} = T_{ST} - \frac{4(Longitude - Local\ Meridian)}{60} + T_{EQ} \qquad [5.9]$$

The declination may be calculated from (Rosenberg et al., 1983)

$$D = 0.4101\cos\left[\frac{2\pi(J - 172)}{365}\right] \qquad [5.10]$$

where J is the day of the year.

Fig. 5.9 Kipp and Zonen model CM-15 albedometer

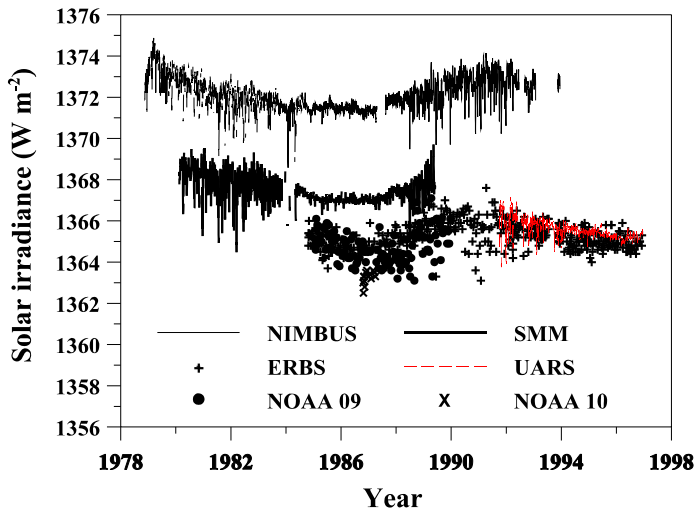

Fig. 5.10 Satellite observations of solar irradiance (Ra) outside the earth's atmosphere; corrected for earth-sun distance. Data source: NOAA (1997)

List (1971) gave 'equation of time' values to the nearest second for the 1st of each month and every 4 days after that for each month (95 values for the year). The following equation reproduces those values with a maximum error of 6 s, and can be used to estimate T_{EQ} in h for any day of the year.

$$T_{EQ} = b_0 + b_1\sin\left(\frac{J}{P_1}\right) + b_2\cos\left(\frac{J}{P_1}\right) + c_1\sin\left(\frac{J}{P_4}\right) + c_2\cos\left(\frac{J}{P_4}\right) + c_3\sin\left(\frac{2J}{P_4}\right) + c_4\cos\left(\frac{2J}{P_4}\right) + c_5\sin\left(\frac{3J}{P_4}\right) + c_6\cos\left(\frac{3J}{P_4}\right) + c_7\sin\left(\frac{4J}{P_4}\right) + c_8\cos\left(\frac{4J}{P_4}\right) \quad [5.11]$$

where the coefficients b_i and c_i are given in Table 5.2, and $P_1 = 182.5/(2\pi)$ and $P_4 = 365/(2\pi)$.

Table 5.2 Coefficients for calculating the 'equation of time' value from Equation [5.11]

b_0	4.744×10^{-5}	c_2	9.19×10^{-3}	c_6	-1.29×10^{-3}
b_1	-0.157	c_3	-5.78×10^{-4}	c_7	-3.23×10^{-3}
b_2	-0.0508	c_4	3.61×10^{-4}	c_8	-2.1×10^{-3}
c_1	-0.122	c_5	-5.48×10^{-3}		

Jensen et al. (1990) gave a simpler method for T_{EQ}

$$T_{EQ} = 0.1645 \sin(2b) - 0.1255 \cos(b) - 0.025 \sin(b) \quad [5.12]$$

where $b = 2\pi(J - 81)/364$. The maximum error compared against List's T_{EQ} values is 88 s.

Disregarding air quality, solar irradiance is affected by latitude, time of year and day, and elevation. Latitude and time affect the sun angle, β, and thus affect both the path length of radiation through the atmosphere (and thus absorption and scattering losses), and the flux density at the surface through Equation

[5.5]. Elevation affects the path length. Methods for calculating extraterrestrial, Rsa, and clear-sky solar irradiance at the surface, Rso, are given by Campbell (1977, Chapter 5), Jensen et al. (1990, Appendix B), Jones (1992, Appendix 7), and McCullough and Porter (1971). Calculation of Rsa depends on latitude and time of day. Once Rsa is calculated, Rso may be estimated from considerations of adsorbtion and scattering in the atmosphere, which depend mainly on the pathlength through the atmosphere and its density. Thus latitude, time of day and elevation are factors in estimating Rso from Rsa. The value of Rso is an important quantity against which to check measured Rsi; and it can be used in estimates of Rn, either to replace Rsi in Equation [5.2], or using regression relationships of Rn = f(Rso) (see Jensen et al., 1990, Appendix B). Duffie and Beckman (1991) presented the following method of calculating Rsa (MJ m^{-2} h^{-1}) for any period, P (h)

$$Rsa = \left[\frac{24(60)}{2\pi}\right] G_{SC} d_r \{\cos(L)\cos(D)[\sin(\omega_2) - \sin(\omega_1)] + (\omega_1 - \omega_2)\sin(L)\sin(D)\} \quad [5.13]$$

where G_{SC} is the solar constant (0.08202 MJ m^{-2} min^{-1}), d_r is the relative earth-sun distance, and ω_1 and ω_2 are the solar time angles at the beginning and end of the period, respectively (all angles in radians). The term $24(60)/(2\pi)$ is the inverse angle of rotation per minute. The relative earth-sun distance is given by

$$d_r = 1 + 0.033\cos\left(\frac{2\pi J}{365}\right) \quad [5.14]$$

where J is the day of year. The factors ω_1 and ω_2 are the solar time angles at the beginning and end of the period in question

$$\omega_1 = \omega - \frac{\pi P}{24} \quad [5.15]$$

$$\omega_2 = \omega + \frac{\pi P}{24} \quad [5.16]$$

where ω is the solar time angle at the center of the period (radians), and P is the length of the period in h.

The sunset time angle (angle from noon to sunset) is given by

$$\omega_s = \cos^{-1}[-\tan(L)\tan(D)] \quad [5.17]$$

from which it is clear that day length, T_D (h), is

$$T_D = \frac{24 w_S}{\pi} \quad [5.18]$$

Equation [5.13] can be re-written for total daily Rsa as

$$Rsa = \left[\frac{24(60)}{2\pi}\right] G_{SC} d_r [\cos(L)\cos(D)\sin(\omega_s) + \omega_s \sin(L)\sin(D)] \quad [5.19]$$

For example, on day 119 at latitude 35° 11′ N, longitude 102° 6′ W, Rsa calculated using Equation [5.13] on a half-hourly basis was 38.097 MJ m^{-2} compared with 38.100 MJ m^{-2} calculated with Equation [5.19].

Jensen et al. (1990) recommended estimating daily total clear sky solar irradiance as

$$\text{Rso} = 0.75\ \text{Rsa} \qquad [5.20]$$

Somewhat in agreement with this, Monteith and Unsworth (1990) stated that direct beam radiation rarely exceeded 1030 W m^{-2}, about 75% of the solar constant.

Jones (1992) and Monteith and Unsworth (1990) suggest

$$Rsi = Rsi_{max} \sin\left(\frac{\pi t}{N}\right) \qquad [5.21]$$

for instantaneous values of Rsi on clear days, where Rsi_{max} is the maximum instantaneous irradiance occurring at solar noon, t is time after sunrise (h), and N is daylength (h).

It is more common to know daily total Rsi. Collares-Pereira and Rabl (1979) gave the ratio of hourly irradiance, Rsi,h to daily irradiance, Rsi,d as

$$\frac{Rsi,h}{Rsi,d} = \left(\frac{\pi}{24}\right)[a + b\cos(\omega)]\frac{\cos(\omega) - \cos(\omega_s)}{\sin(\omega_s) - \omega_s\cos(\omega_s)} \qquad [5.22a]$$

where

$$a = 0.409 + 0.5016\sin\left(\omega_s - \frac{\pi}{3}\right) \qquad [5.22b]$$

and

$$b = 0.6609 - 0.4767\sin\left(\omega_s - \frac{\pi}{3}\right) \qquad [5.22c]$$

Equation [5.22] performed well when applied to data from Bushland, Texas (Fig. 5.11).

More complex methods of estimating Rso account for attenuation of direct beam radiation using Beer's law; coupled with Lambert's law to calculate irradiance on a horizontal surface; plus an accounting of diffuse irradiance (See for example: Jones, 1990; Rosenberg et al., 1983; List, 1971). Beer's law describes the intensity I of radiation after passing a distance x through a medium in terms of an extinction coefficient, k, and the initial intensity, Ia, as

$$I = Ia\ e^{kx} \qquad [5.23]$$

For solar radiation the distance is expressed in terms of air mass number, m, as (List, 1971)

$$m = \sec\left(\frac{\pi}{2} - \beta\right) \qquad [5.24]$$

The air mass is referenced to the length of the path when the sun is directly overhead. For β less than 0.175 radians (10°) the measured air mass number is less than that given by Equation [5.24] due to refraction and reflection at these low angles. List (1971) gives corrections; and notes also that for pressures, p, less than

standard sea-level pressure, p_0, that m should be corrected by $m = m(p/p_0)$. Re-writing Equation [5.23] we have

$$Io = Ia\ e^{k \sec(\pi/2 - \beta)} \qquad [5.25]$$

where Io is direct beam radiation at the earth's surface. Monteith and Unsworth give a range of values of k for England as 0.07 for very clean air to 0.6 for very polluted air.

Assuming that both direct, Io, and diffuse, Id, radiation are known, the total irradiance at the surface is

$$Rsi = Io(\sin\beta) + Id \qquad [5.26]$$

Diffuse radiation is quite difficult to estimate because it is so dependent on cloud cover, and aerosol concentration in the air. Yet, summarizing several data sets, Spitters et al. (1986) found that the proportion of Rd to Rsi is a function of the ratio of Rsi to Rsa (Fig. 5.12) described for daily total Rsi by

$$Rd,d = 1, \qquad Rsi,d/Rsa,d < 0.07 \qquad [5.27a]$$
$$Rd,d/Rsi,d = 1 - 2.3(Rsi,d/Rsa,d - 0.07)^2, \qquad 0.07 \le Rsi,d/Rsa,d < 0.35 \qquad [5.27b]$$
$$Rd,d/Rsi,d = 1.33 - 1.46(Rsi,d/Rsa,d), \qquad 0.35 \le Rsi,d/Rsa,d < 0.75 \qquad [5.27c]$$
$$Rd,d/Rsi,d = 0.23(Rsi,d/Rsa,d), \qquad 0.75 \le Rsi,d/Rsa,d \qquad [5.27d]$$

and for hourly values by

$$Rd,h = 1, \qquad Rsi,h/Rsa,h \le 0.22 \qquad [5.28a]$$
$$Rd,h/Rsi,h = 1 - 6.4(Rsi,h/Rsa,h - 0.22)^2, \qquad 0.22 < Rsi,h/Rsa,h \le 0.35 \qquad [5.28b]$$
$$Rd,h/Rsi,h = 1.47 - 1.66(Rsi,h/Rsa,h), \qquad 0.35 < Rsi,h/Rsa,h \le K \qquad [5.28c]$$
$$Rd,h/Rsi,h = R, \qquad K < Rsi,h/Rsa,h \qquad [5.28d]$$

where

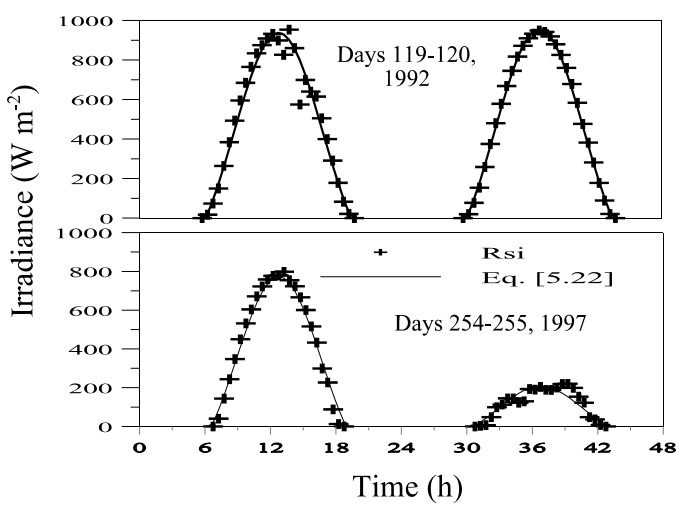

Fig. 5.11 Solar irradiance measured at Bushland, TX in 1992 and 1997 on clear and cloudy days; and Equation [5.22] half-hourly predictions

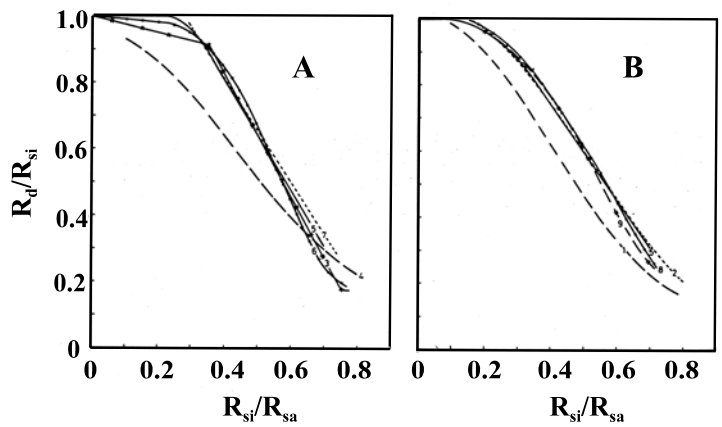

Fig. 5.12 Daily (A) and hourly (B) relationships between Rd/Rsi and Rsi/Rsa [Reprinted from Spitters et al., 1986. Agric. Forest Meteorol. 38:217-229 with kind permission of Elsevier Science - NL, Amsterdam, Netherlands]

$$R = 0.847 - 1.61\sin\beta + 1.04\sin^2\beta \qquad [5.29]$$

and

$$K = \frac{(1.47 - R)}{1.66} \qquad [5.30]$$

5.2.1.3 Surface Albedo and Emissivity

Because Rsi provides most of the energy that is partitioned at the earth's surface, albedo plays a major role in the energy balance. The mean albedo of the earth is 0.36 ± 0.06 (Weast, 1982). But albedo varies diurnally (Fig. 5.13) with higher albedo corresponding to lower sun angle (see also bare soil data of Monteith and Sziecz, 1961, 1992; Idso et al., 1974; and Aase and Idso, 1975). Soil and plant surfaces are often considered optically rough, but in some cases specular (mirror-like) rather than diffuse reflection may occur. Some plant leaves are shiny and reflect specularly when the angle of incident radiation is low. Wet soil surfaces may also reflect specularly. These mechanisms lead to higher albedo when sun angle is low. The albedo of plant stands is also lower in midday because more sunlight penetrates deeply within the canopy and is trapped by multiple reflections. Wilting and other physiological changes during the day may also contribute to changes in albedo.

Soil albedo decreases as water content increases. Bowers and Hanks (1965) found the relationship to be curvilinear; as did Skidmore et al. (1975). Idso and Reginato (1974) found that bare soil albedo changed linearly with water content of the surface 2 mm of soil (smooth clay loam) (Fig. 5.14). For thicker layers the relationship was curvilinear. The maximum albedo, 0.3, occurred for air dry soil, but the minimum albedo, 0.14, occurred at about 0.23 m^3 m^{-3} water content, well before the soil was saturated. This represents field capacity (soil water tension of 30 kPa) for this soil, and Idso and Reginato (1974) postulated that the minimum albedo would occur at field capacity for all soils. Kondo et al. (1992) found a similar relationship for a bare loam with a maximum albedo of 0.24 and minimum of 0.13; and with the minimum attained when soil water content reached about 0.22 m^3 m^{-3}. Data of Idso et al. (1974, 1975) show that the difference in wet and dry soil albedos was constant despite time of day and day of year. Monteith (1961) measured albedo of clay loam to be 0.18 when dry, decreasing to 0.11 when at field capacity water content of 0.35 m^3 m^{-3}

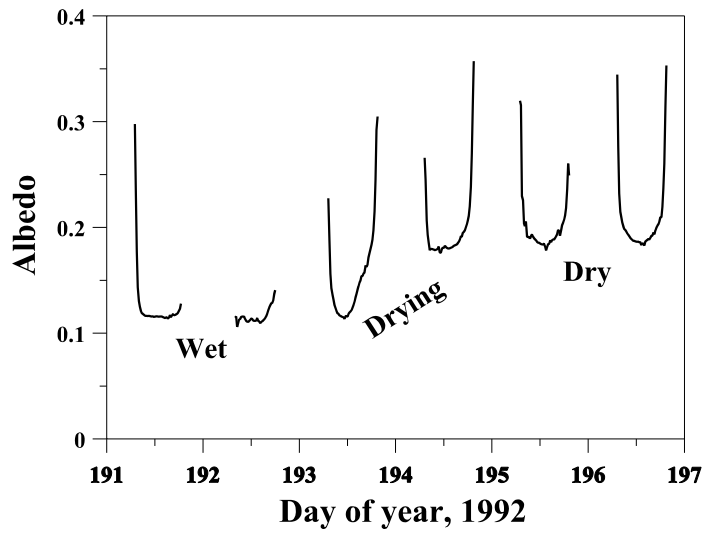

Fig. 5.13 Albedo for smooth, bare Pullman clay loam at Bushland, TX when wet and dry.

The interaction of sun angle and soil drying causes complex patterns of soil albedo change over time. Figure 5.13 illustrates low daytime wet soil albedos of 0.11 after irrigation and rain on days 191 and 192, 1992. Rapid soil surface drying on day 193 caused albedo to rise sharply during the day. Additional drying on day 194 completed the change, and diurnal albedo changes on days 195 and 196 reflected only sun angle effects, with a minimum albedo of 0.2 for this smooth soil surface. The same surface in a roughened condition earlier in the year never reached mid day albedo values higher than 0.13..

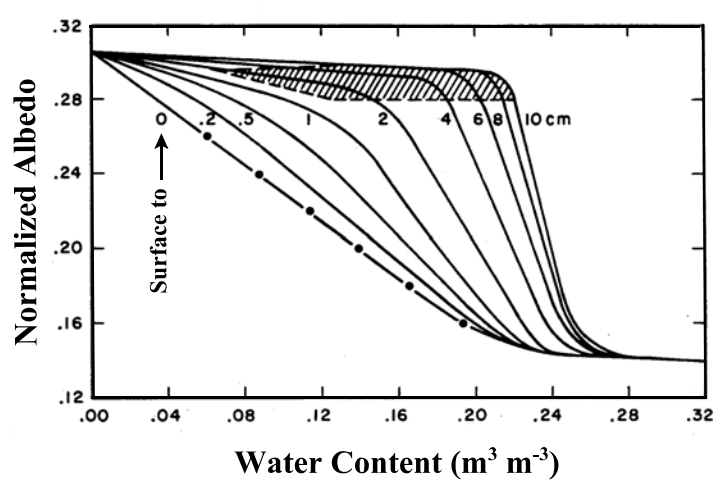

Fig. 5.14 Albedo, normalized according to sun angle, vs. soil water content for different surface layer thicknesses of Avondale clay loam at Phoeniz, AZ. Data for shaded areas are uncertain. From Idso et. al. (1974)

Other than water content, major determinants of soil albedo are color, texture, organic matter content, and surface roughness. Dvoracek and Hannabas (1990) presented a model of albedo dependence on sun angle, surface roughness, and color

$$\alpha = p^{(c \text{ SIN } \beta + 1)} \qquad [5.31]$$

where p was a color coefficient, c was a roughness coefficient, and β is solar angle. They demonstrated good fits with measured data (Table 5.3). Albedo values modeled using p and c values from Table 5.3 for wheat and cotton (day of year 192, latitude 41°N) appear realistic (Fig. 5.15). However, the physical meaning of the p and c coefficients is not well understood.

Table 5.3 Color (p) and roughness (c) coefficients for Equation [5.31]. [Modified from Dvoracek and Hannabas. 1990. Proc. 3rd Nat. Irrig. Symp., Phoenix, AZ with permission of American Society of Agricultural Engineers]

Surface and condition	Color coefficent p	Roughness coefficient c	Mean r^2
Lakes and ponds, clear water			
waves, none	0.13	0.29	0.82
waves, ripples up to 2.5 cm	0.16	0.70	0.74
waves, larger than 2.5 cm with occasional whitecaps	0.23	1.25	0.83
waves, frequent whitecaps	0.30	2.00	0.85
Lakes and ponds,			
green water, ripples up to 2.5 cm	0.22	0.70	0.90
muddy water, no waves	0.19	0.29	0.76
Cotton			
winds, calm to 4.5 m s^{-1}	0.27	0.27	0.80
winds, over 4.5 m s^{-1}	0.27	0.43	0.88
Wheat			
winds, calm to 4.5 m s^{-1}	0.31	0.92	0.85
winds, over 4.5 m s^{-1}	0.37	1.30	0.85

Daily mean albedos may be calculated as the ratio of daily total reflected shortwave energy to daily total Rsi. Using data from Figs. 5.5 and 5.6, daily mean albedos for fallow (soybean residue) and alfalfa differ by about 0.10 when the soil is very dry (Fig. 5.16). The gradual decline in fallow albedo in early 1996 may be due to decomposition of the soybean residue. Albedo for the alfalfa field declined at each cutting to nearly that of the fallow field, which was initially rougher than the soil under the alfalfa. But, during heavy rains in the latter part of the year, the fallow soil surface was slaked and smoothed and its albedo increased to near that of the alfalfa. Thus, after the 4th cut the alfalfa field albedo was lower than that of the fallow field for a brief time, probably because the alfalfa was irrigated and the fallow field had dried out again. Peaks of albedo exceeding 0.8 were due to snow early and late in the year. In contrast to soil, albedo of closed canopies (well watered) is relatively constant (Table 5.4).

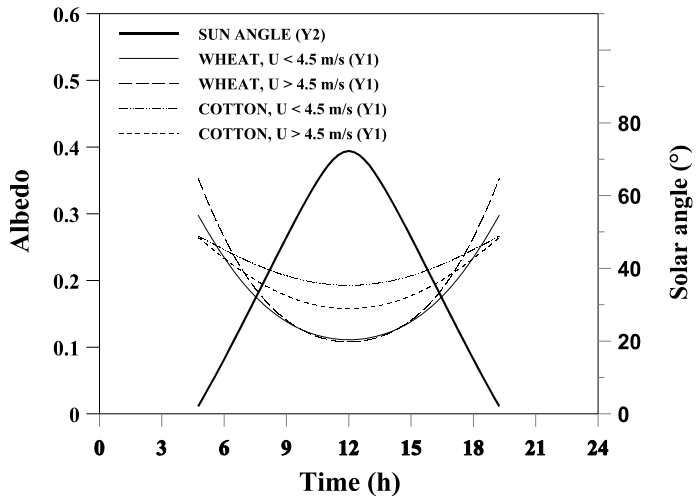

Fig. 5.15 Albedo for wheat and cotton from Equation [5.31]

Albedo values for many plant covers may be found in Gates (1980). For surfaces with plants, the amount of radiation reaching the soil surface, Rt (Fig. 5.1), depends on the leaf area index (LAI) and the canopy structure. Numerical models have been developed that take into account leaf orientation and distribution in the canopy to calculate absorption of radiation at different levels in the canopy (Goudriaan, 1977; Chen, 1984). Lascano et al. (1987) used Chen's model to calculate polynomials representing the dependence of albedo on LAI, as well as the dependence of the view factor (proportion of sky visible from the soil) on LAI; and incorporated these into their ENergy and WATer BALance model (ENWATBAL) . Monteith and Unsworth (1990) present equations describing the albedo of a deep canopy with a spherical distribution of leaves for sun angles higher than 25°. More discussion of these concepts can be found in Russell et al. (1989). For field studies we can either measure albedo, or directly measure the components of net radiation, or use a net radiometer (Table 5.1). The transmitted radiation can be measured below the canopy with tube solarimeters.

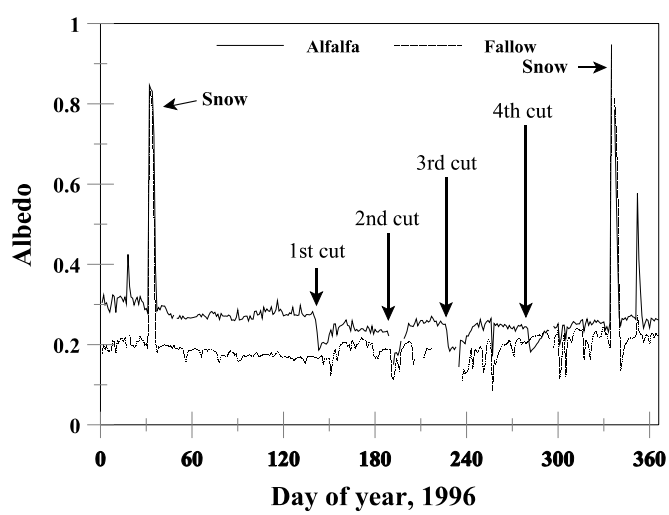

Fig. 5.16 Daily mean albedos for irrigated alfalfa, and fallow after soybean on Pullman clay loam at Bushland, TX

Table 5.4 Some Albedo and Emissivity Values for Various Soil and Plant Surfaces.

Surface	Albedo	Emissivity	Source
soils, dark, wet to light, dry	0.05-0.50	0.90-0.98	Oke, 1978
dry sandy soil	0.25-0.45		Rosenberg et al., 1983
bare dark soil	0.16-0.17		"
dry clay soil	0.20-0.35		"
quartz sand	0.35		van Wijk and Scholte Ubing, 1963
sand, wet	0.09	0.98	"
sand, dry	0.18	0.95	"
dark clay, wet	0.02-0.08	0.97	"
dark clay, dry	0.16	0.95	"
fields, bare	0.12-0.25		"
fields, wet, plowed	0.05-0.14		"
dry salt cover	0.50		"
snow, fresh	0.80-0.95		Rosenberg et al., 1983
snow, old	0.42-0.70		"
snow, fresh	0.95	0.99	Oke, 1978
snow, old	0.40	0.82	"
snow, fresh	0.80-0.85		van Wijk and Scholte Ubing, 1963
snow, compressed	0.70		"
snow, melting	0.30-0.65		"
grass, long (1 m)	0.16	0.90	Oke, 1978
short (0.02 m)	0.26	0.95	"
grass, green	0.16-0.27	0.96-0.98	van Wijk and Scholte Ubing, 1963
grass, dried	0.16-0.19		"
prairie, wet	0.22		"
prairie, dry	0.32		"
stubble fields	0.15-0.17		"
grain crops	0.10-0.25		"
green field crops full cover, LAI>3	0.20-0.25		Jensen et al., 1990
leaves of common farm crops		0.94-0.98	Jensen et al., 1990
most field crops	0.18-0.30		Rosenberg et al., 1983
field crops, latitude 22-52°	0.22-0.26	0.94-0.99	Monteith and Unsworth, 1990
field crops, latitude 7-22°	0.15-0.21	0.94-0.99	"
deciduous forest	0.15-0.20	0.96†	Rosenberg et al., 1983
decid. forest, bare	0.15	0.97	Oke, 1978
leaved	0.20	0.98	Oke, 1978
coniferous forest	0.10-0.15	0.97[1]	Rosenberg et al., 1983
coniferous forest	0.05-0.15	0.98-0.99	Oke, 1978
vineyard	0.18-0.19		Rosenberg et al., 1983
mangrove swamp	0.15		"
grass	0.24		Jones, 1992
crops	0.15-0.26		"
forest	0.12-0.18		"
water, high sun	0.03-0.10	0.92-0.97	Oke, 1978
water, low sun	0.10-1.00	0.92-0.97	"
sea, calm	0.07-0.08		Rosenberg et al., 1983
sea, windy	0.12-0.14		"
ice, sea	0.30-0.45	0.92-0.97	Oke, 1978
ice, glacier	0.20-0.40		
ice, lake, clear	0.10		Rosenberg et al., 1983
ice, lake, w/ snow	0.46		"

† van Wijk and Scholte Ubing, 1963

Example 5.1: Spectral Reflection and Radiation.

The discussion of emissivities and albedos of surfaces given here is based on a broadband view of irradiance, reflection, and emission that recognizes only short-wave and long-wave radiation as presented in Fig. 5.7. Although these are arguably the most important features from an energy balance perspective, there is much recent work on multi-spectral sensing of radiation reflected and emitted from vegetation and soil surfaces (Robert et al., 1999). This spectral sensing may be done for only a few relatively narrow bands of radiation in the visible and infrared, or may involve hyperspectral scanning that provides sensing of radiation for every nm of the spectrum across a wide range. The advent of fiber optics capable of transmitting both visible and infrared light and the development of miniaturized spectrometers (for example, the Ocean Optics, Inc. model S2000) has revolutionized the way that researchers view plant and soil surfaces.

An example of multi-spectral sensing is the use of red and near infrared (NIR) reflectance from a cotton canopy (Fig. 5B.1). The ratio of NIR/Red reflectances is clearly related to leaf area index. However, the relationship is not stable from year to year and research continues. Other uses include sensing of the onset and progression of plant disease and insect infestation, and sensing of plant water status. Much work remains to be done to make these techniques useful.

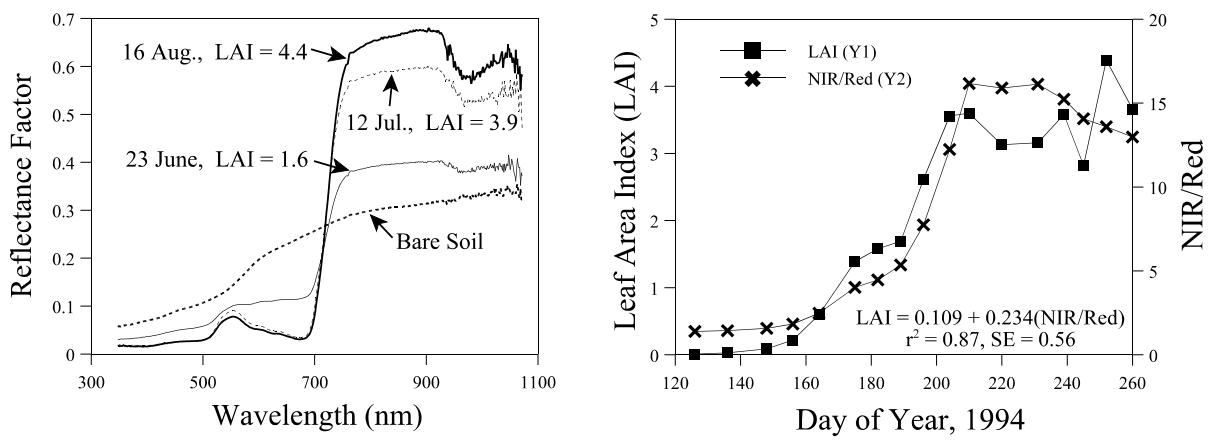

Fig. 5B.1 Reflectance factor vs. wavelength for bare soil and cotton at three levels of leaf area index (LAI) (left), and the relationship between the ratio of near infrared to red reflectance and LAI (right) for cotton in Arizona. Personal communication from Paul J. Pinter, Jr. and Edward M. Barnes, U.S. Water Conservation Laboratory, USDA-ARS, Phoenix, AZ, May 2000.

5.2.1.4 Incoming Long Wave Radiation

Methods of estimating long wave irradiance from the sky, L↓, usually take the form

$$L\downarrow = \epsilon\sigma(T_a + 273.16)^4 \qquad [5.32]$$

where T_a (°C) is air temperature at the reference measurement level (often 2 m), and the emissivity (ϵ) may be estimated from the vapor pressure of water in air at reference level (e_a) (kPa), or using both e_a and T_a. The vapor pressure is

$$e_a = RH(e_s) \quad [5.33]$$

where RH is the relative humidity of the air and e_s is the saturation vapor pressure (kPa) at T_a (°C) given by (Murray, 1967).

$$e_s = 0.61078 \exp\left(\frac{17.269\,T_a}{237.3 + T_a}\right) \quad [5.34]$$

If the dew point temperature, rather than the RH, is known then

$$e_a = 0.61078 \exp\left(\frac{17.269\,T_{dew}}{237.3 + T_{dew}}\right) \quad [5.35]$$

Hatfield et al. (1983) compared several methods for estimating ϵ and concluded that methods using only air temperature performed less well than those that used vapor pressure or both vapor pressure and air temperature.. Among the best methods was Idso's (1981) equation

$$\epsilon_a = 0.70 + 5.95 \times 10^{-4} e_a \exp\left(\frac{1500}{T_a + 273.1}\right) \quad [5.36]$$

where e_a is in kPa. Idso showed fairly conclusively that ϵ is a function of both e_a and T_a.

Howell et al. (1993) measured L↓ (Table 5.1) and calculated ϵ by inverting Equation [5.32]. Applying Equation [5.36] as well as Brunt's (1932) equation

$$\epsilon_a = 0.52 + 0.206 e_a^{0.5} \quad [5.37]$$

and Brutsaert's (1982) equation

$$\epsilon_a = 0.767 e_a^{1/7} \quad [5.38]$$

to their data shows that all three equations gave good predictions for clear sky conditions but probably underestimated ϵ for cloudy and nighttime conditions (Fig. 5.17). For regressions of predicted vs. measured ϵ, the Idso equation gave a slightly higher correlation coefficient and a slope closer to unity (Table 5.5). Under heavy clouds sky emissivity approaches unity, and none of these models predicts this well.

Despite the difficulty of estimating sky emissivity well, uncertainty in the value of L↓ usually causes little difficulty in estimating net radiation because L↓ is very often a small component of the energy balance.

Table 5.5 Regressions of predicted emissivity (ϵ_p) vs. measured values (ϵ) for data from day 133 through 140 and 192 through 197, 1992 at Bushland, TX.

Method	Regression Equation	r^2	SE
Brunt, Equation [5.37]	$\epsilon_p = 0.505 + 0.325\epsilon$	0.33	0.024
Brutsaert, Equation [5.38]	$\epsilon_p = 0.556 + 0.311\epsilon$	0.32	0.024
Idso, Equation [5.36]	$\epsilon_p = 0.522 + 0.398\epsilon$	0.37	0.027

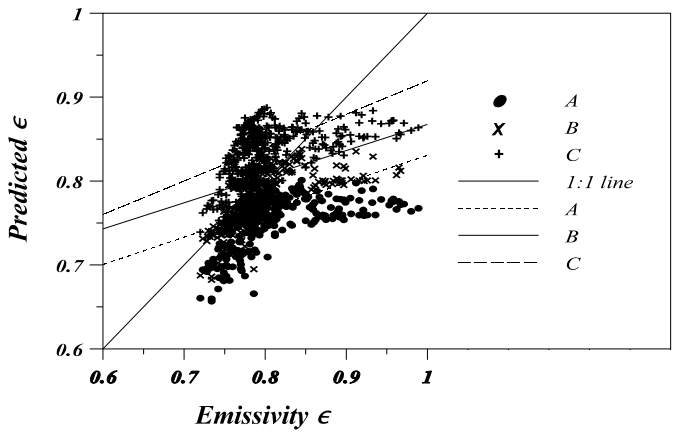

Fig. 5.17. Comparison of predictions with measured emissivity for two periods in 1992 at Bushland, TX. Points plotted at extreme right were associated with nighttime and overcast conditions. A = Equation [5.37], B = Equation [5.38], C = Equation [5.35]. Lines are for regressions shown in Table 5.5

5.2.1.5 Comparison of Net Radiation Estimates with Measured Values

It has become commonplace to have data from field weather stations that includes Rsi; and air temperature, T_{az}, wind speed, U_z, and relative humdity, RH_z, measured at some reference height, z, (often 2 m). Measurement of Rn is still not common, probably due to several factors including additional expense, fragility of the plastic domes used on some models of net radiometer, and problems with calibration. Net radiometer calibration changes with time, and experience shows that even new radiometers may not agree within 10%. If a net radiometer is used, it is prudent, as with all instruments, to check measured Rn values against estimated ones. Methods presented in previous sections can be used to estimate Rn, but simpler methods exist that are adequate for most cases. Jensen et al. (1990) compared four methods of estimating Rn, including Wright and Jensen (1972), Doorenbos and Pruitt (1977), a combination of Brutsaert (1975) and Weiss (1982), and Wright (1982), against values measured at Copenhagen, Denmark, and Davis, California. The Wright (1982) method was overall best, but underestimated Rn in the peak month at Copenhagen by 9%. The Wright and Jensen (1972) method was almost as good. These methods all assume that surface temperature is not measured, so that only air temperature is used in the calculations.

Jensen et al. (1990) calculated net long wave radiation, Rnl, as

$$Rnl = -\left[a\left(\frac{Rsi}{Rso}\right) + b\right]\left(a_1 + b_1 e_d^{0.5}\right)\sigma T_{az}^4 \qquad [5.39]$$

where e_d is the saturation vapor pressure of water in air at dew point temperature (kPa); and the term $(a_1 + b_1 e_d^{0.5})$ is a 'net emittance', ϵ', of the surface. The 'net emittance' attempts to compensate for the fact that surface temperature is not measured, the assumption being that T_{az} can substitute reasonably well for both sky and surface temperature. The coefficients a, b, a_1, and b_1 are climate specific; a and b being cloudiness factors. Some values are presented by Jensen et al. (1990, Table 3.3).

Many weather stations report only daily totals of solar radiation; and maximum and minimum of air temperature, T_x and T_n, respectively (K). If this is the case, the term σT^4 can be estimated as

$$\sigma T^4 \cong \sigma(T_x^4 - T_n^4)/2 \qquad [5.40]$$

If mean dew point temperature is not available it may be estimated as equal to T_n in humid areas.

Allen et al. (1994a,b) presented slightly modified versions of the methods presented by Jensen et al. (1990) in a proposed FAO standard for reference evapotranspiration estimation. As an example, estimates of daily total net radiation were made for Bushland, Texas using the following equations from Allen et al. (1990)

$$Rn = (1 - \alpha)Rs - \left[a_c\left(\frac{Rsi}{Rso}\right) + b_c\right]\left(a_1 + b_1 e_d^{0.5}\right)\sigma\left(\frac{T_m^4 + T_n^4}{2}\right) \qquad [5.41]$$

where the cloud factors were a_c = 1.35 and b_c = -0.35, the emissivity factors were a_1 = 0.35 and b_1 = -0.14, the albedo was α = 0.23, Rsi was measured, e_d was calculated from mean dew point temperature, and Rso was calculated from

$$\text{Rso} = (.75 + .00002\ \text{ELEV})\text{Rsa} \qquad [5.42]$$

where Rsa is from Equation [5.19], and ELEV is elevation (m) above mean sea level. This is similar to Equation [5.20] but with a correction increasing Rso for higher elevation sites. The mean daily saturated vapor pressure at dew point temperature was estimated from mean daily dew point temperature, T_d

$$e_d = 0.611 \exp\left(\frac{17.27 T_d}{237.3 + T_d}\right) \qquad [5.43]$$

Additional estimates were calculated from half-hourly measured values of Rsi, T_a, and T_d using equations given by Allen et al. (1994) equivalent to Equations [5.7], [5.8], [5.10], [5.12], [5.13], [5.14], [5.15], and [5.16] to estimate half-hourly Rsa, and Equation [5.41] to estimate half-hourly Rso. Equation [5.42] was applied to half-hourly dew point temperatures to estimate half-hourly e_d values. Equation [5.40] was written for half-hourly values of air temperature, T_a, as

$$Rn = (1 - \alpha)Rs - \left[a_c\left(\frac{Rsi}{Rso}\right) + b_c\right]\left(a_1 + b_1 e_d^{0.5}\right)\sigma T_a^4 \qquad [5.44]$$

where the ratio of Rsi to Rso was set to 0.7 for nighttime estimates of Rn.

Comparison of daily Rn estimates, calculated using half-hourly data means, with measurements made with a REBS Q*5 (Seattle, WA) net radiometer over irrigated grass show excellent agreement for alfalfa (Fig. 5.18) and grass (Fig. 5.19) at Bushland, TX. But, there was a consistent bias for Rn estimated from daily means, with underestimation of Rn at high measured values, and overestimation at low measured values (Fig. 5.20). The bias evident when daily means and maximum/minimum temperatures were used is probably tied to both poor estimates of vapor pressure from the max/min temperature data; and the inadequacy of Equation [5.39].

Estimates of half-hourly net radiation for alfalfa at Bushland, Texas using half-hourly data and these methods also gave good results (Fig. 5.21). Allen et al. (1994a, b) give detailed methods for estimating Rn when measurements are missing for Rsi and/or e_d.

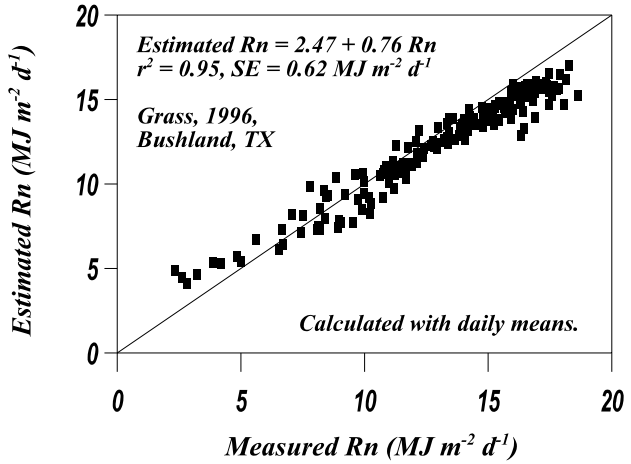

Fig. 5.18 Daily net radiation, estimated with methods from Allen et al. (1994ab) using daily means and maxima and minima, compared with measurements with a REBS Q*5 net radiometer over drip irrigated grass in 1996 at Bushland, TX

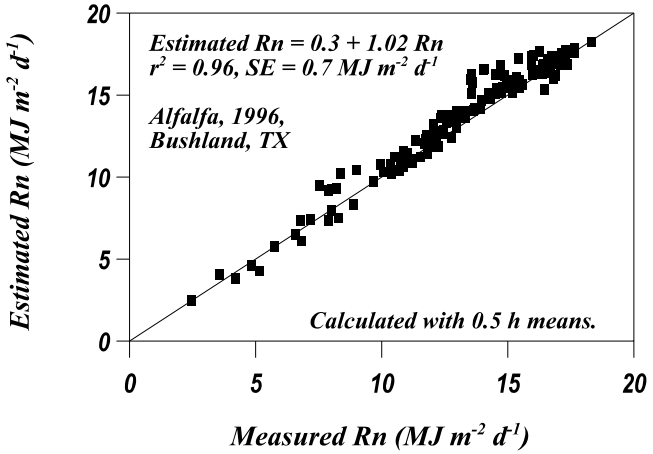

Fig. 5.19. Net radiation estimated with methods from Allen et al. (1994ab) compared with measurements over sprinkler irrigated alfalfa in 1996 at Bushland, TX

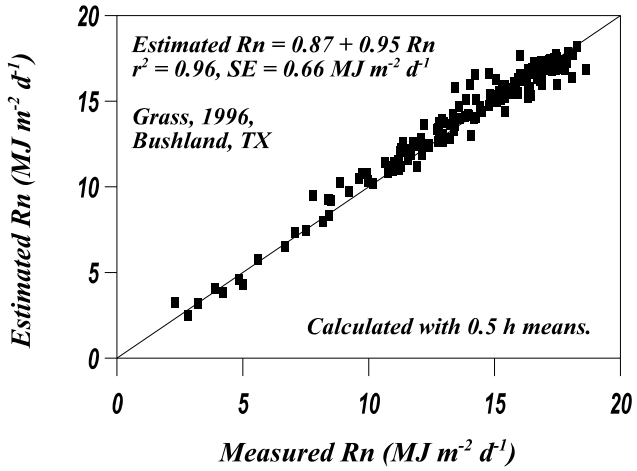

Fig. 5.20. Daily net radiation, estimated with methods of Allen et al. (1994ab) using half-hourly data, compared with measurements with a REBS Q*5 net radiometer over drip irrigated grass in 1996 at Bushland, TX.

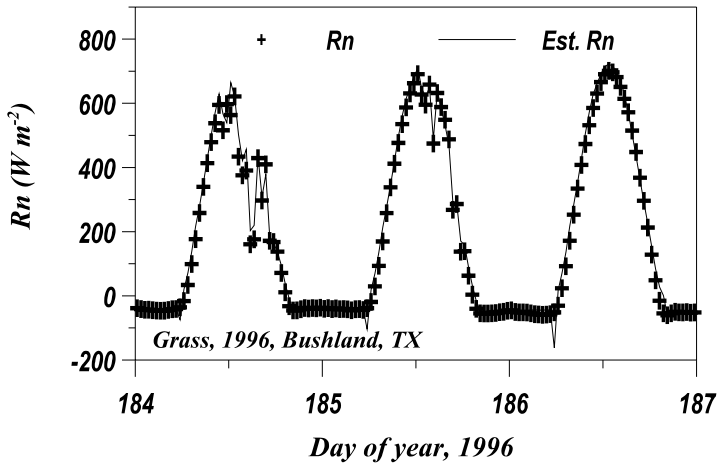

Fig. 5.21 Half-hourly measured net radiation compared with values estimated with methods of Allen et al. (1994ab) using half-hourly data for drip irrigated grass at Bushland, TX, 1996.

5.2.2 Latent Heat Flux Measurement

Latent heat flux is the product of the evaporative flux, E (kg s^{-1} m^{-2}), and the latent heat of evaporation, L (2.44 x 10^6 J kg^{-1} at 25 °C). The value of L is temperature dependent, but is well described (in J kg^{-1} x 10^6) by

$$L = 2.501 - 2.370 \times 10^{-3}T \qquad (r^2 = 0.99995) \qquad [5.45]$$

where T is in °C. Methods of measurement of E include weighing lysimeter (including microlysimeters), and other mass balance techniques that rely on measurements of change in soil water storage, ΔS, as well as eddy correlation and Bowen ratio measurements. Because ΔS is a component of the soil water balance, and lysimetry is a key tool for investigations of soil water balance, discussion of lysimetric techniques will be deferred to section 5.2.

5.2.2.1 Boundary Layers

Evaporative fluxes move between plant, or soil, surfaces and the air by both diffusion and convection. Diffusive processes prevail in the laminar sublayer close (millimeters) to these surfaces. In this layer air movement is parallel to the surface and little mixing occurs. Vapor flux across the laminar sublayer is well described by a Fickian diffusion law relating flux rate to vapor pressure gradient factored by a conductance term. But in the turbulent layer beyond the laminar layer the flux is mostly convective in nature so that water vapor is moved in parcels of air that are moved and mixed into the atmosphere in turbulent flow. These moving parcels of air are often referred to as eddies, similar to eddies seen in a stream. Usually the eddies are not visible, but in foggy, smoky or dusty air they may be apparent. Certainly anyone who has felt the buffeting of the wind can attest to the force of eddies and the turbulence of the air stream in which they occur. As wind speeds increase the depth of the laminar sublayer decreases. Surface roughness enhances this process, resulting in thinner laminar sublayers. Because the resistance to vapor transport across the laminar airstream is much larger than the resistance across a turbulent airstream of similar dimension, increasing

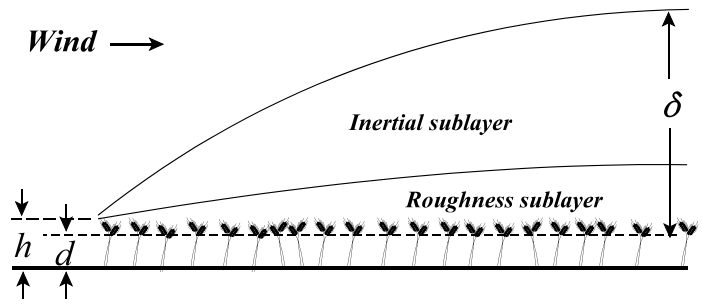

Fig. 5.22 Schematic of sublayers of the surface boundary layer over a wheat crop. The height (h) of the crop, and the depth (δ) of the constant flux layer are noted. The height (d) is the zero plane displacement height, which is the height to which a logarithmic wind profile, measured above the crop, would extrapolate to zero wind speed.

roughness and wind speed both tend to enhance vapor transport. If the air is still, then eddies due to turbulent flow do not exist, but eddies due to free convection may well be present. Free convection occurs when an air parcel is warmer (or colder) than the surrounding air and thus moves upward (or downward) because it is lighter (or heavier). These buoyancy effects can predominate at very low wind speeds when the surface is considerably warmer than the air. As opposed to free convection, transport in eddies due to wind is called forced convection.

A full discussion of the fluid mechanics of laminar and turbulent flow, Fickian diffusion, and forced and free convection is well beyond the scope of this chapter. Discussions relevant to soil and plant surfaces are presented in Chapters 7-9 of Monteith and Unsworth (1990), Chapters 3 and 4 of Rosenberg et al. (1983), and Chapter 3 of Jones (1992). Here we will concentrate on some results and methods of measurement. These methods are valid within the constant flux layer (Fig. 5.22) which is a layer of moving air which develops from the point at which the air stream first reaches a surface of given condition, for example the wheat field shown in Fig. 5.22. As the air moves over the field it mixes, equilibrating with the new surface condition, and forming a layer of gradually increasing thickness, δ, within which the flux of heat and vapor is constant with height. This is the fully adjusted or equilibrium layer. Within this layer is a layer, extending from the roughness elements (wheat plants in this schema) upward, within which air flow is more turbulent due to the influence of the roughness elements. This is called the roughness sublayer (Monteith and Unsworth, 1990). For any measurement of air temperature, humidity or wind speed, the fetch is the distance upwind from the point of observation to the edge of the new surface. The ratio of the fetch to the value of δ is dependent on the roughness of the surface, the stability of the air, and the wind speed. For many crop surfaces it may be as small as 20:1 or as large as 200:1. For smooth surfaces such as bare soil the ratio may well be larger than 200:1. Measurements should be made in the constant flux layer but above the roughness sublayer.

5.2.2.2 Eddy Correlation Measurements

The observation of turbulent flow and concept of eddies leads to the eddy correlation method of latent heat flux measurement. The main idea here is that if eddies with a vertical velocity component upward are correlated with humidities on average higher than the humidities correlated with downward moving eddies then the net flux of water vapor is upward. In this method very fast response sensors are used to measure the vertical wind speed and humidity simultaneously at a rate of, for example, 20 Hz. This gives a direct measure of the flux at the measurement height (but see fetch requirements below) according to (Rosenberg et al., 1983)

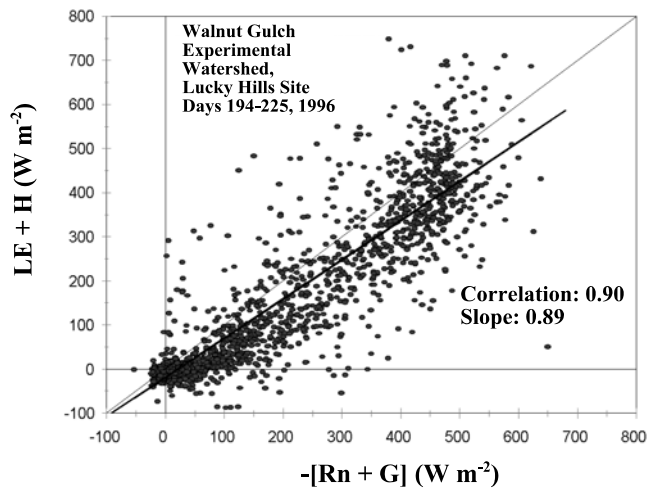

Fig. 5.23. Check of eddy correlation system LE and H values against measured Rn and G values (Adapted from Houser, 1998 with permission)

$$E = \left(\frac{M_w}{M_a P}\right) \rho_a \overline{w' e_a'} \qquad [5.46]$$

where the overscores indicate time averages of vertical wind speed, w′, and vapor pressure, e_a'; the primes indicate instantaneous deviations from the mean; P is atmospheric pressure (Pa), ρ_a is air density; and M_w and M_a are the molecular weights of water and air. The rate of data acquisition must be faster for measurements nearer the surface. Monteith and Unsworth (1992) state that eddy sizes increase with surface roughness and wind speed, and with height above the surface; and they suggest one kHz rates may be needed near a smooth surface, while 10 Hz or slower may be adequate at several meters above a forest. Because the measurements should take place within the fully adjusted boundary layer, simply increasing sensor height will not eliminate the need for fast sensor response. Eddy correlation methods are difficult to carry out due to the data handling and sensor requirements. Data processing requirements are large, but modern data logging and computing equipment are capable of handling these. Commercial systems including data processing software are now available, although expensive (Campbell Scientific Inc., Logan Utah; and The Institute of Ecology and Resource Management at the University of Edinburgh, Scotland). The sonic anemometer is the wind sensor of choice for eddy correlation work due its fast response and sensitivity. At this time a single axis unit costs about $2,500, and a three dimensional sonic anemometer costs about $8,000. Suitable vapor pressure sensors include the krypton hygrometer and infrared gas analyzer (IRGA) available at this writing in the 5 to 10 thousand dollar range.

Eddy correlation measurements may be made for sensible heat flux as well (see section 5.1.4); and if both E and H are measured by eddy correlation the performance of the system may be checked (Houser et al., 1998) by re-arranging Equation [5.1] to

$$LE + H = -Rn - G \qquad [5.47]$$

and measuring Rn and G (Fig. 5.23). Fast response thermocouples for measuring air temperature are used in eddy correlation systems for measuring H. Because these are very much less expensive than fast response vapor pressure sensors, it is sometimes sensible to measure Rn and G, and H by eddy correlation, and find LE as the residual

$$LE = -Rn - G - H \qquad [5.48]$$

Comparisons of eddy correlation and Bowen ratio systems are found in Houser et al. (1998) and Dugas et al. (1991). Some specifics of eddy correlation system design are given in Unland et al. (1996) and Moncrieff et al. (1997).

5.2.2.3 Bowen Ratio Measurement

The Bowen ratio is the ratio of sensible to latent heat flux, $\beta = H/LE$. Introducing this into Equation [5.1] and re-arranging gives the Bowen ratio method for estimating LE

$$LE = \frac{-(Rn + G)}{\beta + 1} \qquad [5.49]$$

In the constant flux layer it is possible to measure temperature and vapor pressure differences at two heights, z_1 and z_2, and evaluate β from a finite difference form

$$\beta = \frac{\dfrac{K_H \rho_a c_p (T_{z_2} - T_{z_1})}{z_2 - z_1}}{\dfrac{K_V \left(\dfrac{\epsilon_m}{P}\right) \rho_a L (e_{z_2} - e_{z_1})}{z_2 - z_1}} \approx \frac{c_p (T_{z_2} - T_{z_1})}{\left(\dfrac{\epsilon_m}{P}\right) L (e_{z_2} - e_{z_1})} = \gamma \frac{(T_{z_2} - T_{z_1})}{(e_{z_2} - e_{z_1})} \qquad [5.50]$$

where the second and third entities assume equivalency of the exchange coefficients for sensible heat flux, K_H, and latent heat flux, K_V; ϵ_m is M_w/M_a; and $\gamma = c_p P/(\epsilon_m L)$ is the psychrometric 'constant'. Commonly, values of T and e are half-hour or hourly means. Because the sensor response time does not have to be very short, Bowen ratio equipment is much less expensive than that for eddy correlation, with complete systems available for under $10,000. Systems are available from Radiation and Energy Balance Systems (REBS), Seattle, WA; Campbell Scientific, Inc., Logan, UT, and others.

Because slight differences in instrument calibration may lead to large errors, it is advisable to switch instruments between the measurement heights. The moving arm system popularized by REBS is one way to do this. Bowen ratio measurements are usually valid only during daylight hours. At night the sum of Rn and G approaches zero causing Equation [5.49] to become imprecise. For periods just after sunrise and before sunset the gradients of T and e may become small at the same time that Rn becomes small, leading to instability in Equation [5.49] and imprecision in the estimate of LE. Under advective conditions Bowen ratio systems tend to underestimate LE when regional sensible heat advection occurs (Todd, 1998b; Blad and Rosenberg, 1974), probably because $K_H/K_V > 1$ under the stable conditions that prevail then (Verma et al., 1978). Four Bowen ratio systems were compared by Dugas et al. (1991) who discuss the merits of different designs. Three eddy correlation systems agreed well with each other; but LE measurements from them were consistently lower than those from the four Bowen ratio systems.

5.2.2.4 Fetch Requirements

Both eddy correlation and Bowen ratio methods are sensitive to upwind conditions. The LE and H values from these methods represent an areal mean for a certain upwind area, often called the 'footprint'. Both methods require considerable upwind fetch, often running to hundreds of meters, of surface that is essentially the same as that where the measurement is made, if the measurement is to be representative of that surface. Also, the longer the same-surface fetch is, the deeper is the fully adjusted layer, and the higher the instruments

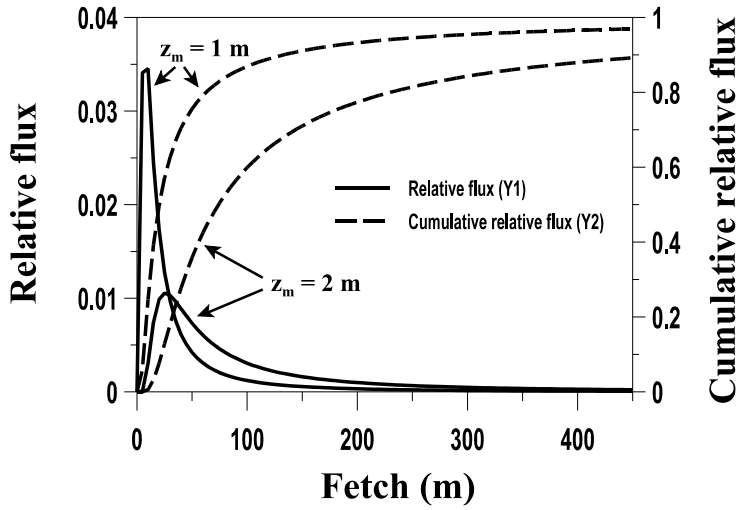

Fig. 5.24 Relative and cumulative relative flux of an alfalfa field for measurement heights (z_m) of 1 and 2 m, moderately stable thermal conditions, and canopy height of 0.5 m. Cumulative relative flux reaches 0.8 at 65 m for z_m = 1 m, and at 225 m for z_m = 2 m.

can be placed above the surface. Issues of instrument height and fetch are discussed by Savage et al. (1995 and 1996) who recommended placing the sonic anemometer no closer than 0.5 m above a short grass cover. Because eddies are smaller nearer the surface, placement of the sonic anemometer too near the surface may lead to eddies being smaller than the measurement window of the anemometer. Fetch requirements may be stated as a ratio of fetch distance to instrument height. Heilman et al. (1989) studied fetch requirements for Bowen ratio systems, and concluded that a fetch ratio of 20:1 was adequate for many measurements, down from the 100:1 ratios reported earlier. Fetch requirements increase as measurement height, z_m, increases. This poses some additional problems for Bowen ratio systems because these incorporate two sensors and the sensors must be separated enough that the vapor pressure and temperature gradients between them are large enough to be accurately sensed. The rougher the surface the smaller the gradients. For many surfaces, and common instrument resolution, these facts lead to separation distances on the order of a meter. The lower measurement should be above the roughness sublayer, typically at least 0.5 m above a crop (more for a very rough surface such as a forest), so the upper measurement may well be nearly 2 m above the crop surface. This could easily lead to a fetch requirement of 100 m. Analysis of relative flux and cumulative relative flux for an alfalfa field under moderately stable conditions using the methods of Schuepp et al. (1990) leads to rather large fetch requirements (Todd, 1998a) (Fig.24). For unstable conditions, mixing is enhanced and the boundary layer becomes adjusted more quickly over a new surface so that fetch requirements are lessened. Fetch requirements are more severe for Bowen ratio than for eddy correlation measurements (Schmid, 1997).

Because of the direct way in which fluxes are measured in eddy correlation schemes, this method is sometimes stated to be the only 'true' measure of latent (or sensible) heat flux. However, consideration of fetch requirements leads to a conclusion that both eddy correlation and Bowen ratio measurements are 'true' only for a constantly changing footprint area upwind of the measurement location. The footprint area and the 'true' flux are poorly defined because the location and size of the footprint change with wind direction and speed. There is strength in this kind of areal averaging, because it reduces noise due to the spatial variability of evaporation. But the measurement cannot be said to be true for any specific location. Indeed, as wind direction changes the measurement area may change completely. By contrast, the soil water balance methods of estimating E, discussed in section 5.2, provide measures for specific locations. In the case of

weighing lysimeters these are in fact direct measurements of E, specific to a well defined location, for all times during which precipitation and runoff are not occurring (neglecting the negligible change in plant mass over short periods).

Example 5.2: Precision Farming Research Tools Needed.

Both eddy correlation and Bowen ratio measurements are based on the assumption that, within the fully adjusted layer, the vertical energy fluxes are uniform with height, i.e., that there is no vertical flux divergence. However, we see from footprint analysis that, for non-zero wind speeds, the upwind area contributes to the measured flux. Even in supposedly uniform fields there is spatial variability in soil properties and plant responses, so that there is almost always some horizontal flux divergence, and therefore necessarily some vertical flux divergence. Although both methods have been described as "point" measurements, they are really averages over an area, with closer upwind sub-areas being weighted more heavily; and with wind speed and atmospheric stability causing changes in the relative weighting of sub-areas and the total area involved. Interest in the spatial variability of the energy balance, particularly the LE component, and in precision farming technologies aimed at addressing crop requirements for water and nutrients at scales well below the field size, has led to a need to measure the spatial variability of LE at scales smaller than can reasonably be addressed with Bowen ratio and eddy correlation systems. As will be discussed in the next box, the radiometric surface temperature can be remotely sensed to give the spatial variability of LE based on Equations [5.1] and [5.73]. However, this approach is weakened by problems with quantifying surface and aerodynamic resistances and discriminating between crop and soil contributions to the radiometric temperature. There remains a need for ground truth measurements giving LE for a well-defined area. The water balance methods discussed in Section 5.3.1 are capable in many cases, but costs of deployment are practically insurmountable. Thus, there remains a need for inexpensive, accurate, unattended soil profile water content measurement methods for implementation of the water balance method of LE measurement.

5.2.2.5 Penman-Monteith Estimates of Latent Heat Flux

Since Penman (1948) published his famous equation describing evaporation from wet surfaces based on the surface energy balance, there have been developments, additions and refinements of the theory too numerous to mention. Notable examples are the van Bavel (1966) formulation, which includes a surface roughness length term, z_0; and the Penman-Monteith (PM) formula (Monteith, 1965), which includes aerodynamic and surface resistances. The van Bavel equation tends to overestimate in windy conditions and is very sensitive to the value of z_0 (Rosenberg, 1969). Howell et al. (1994) compared several ET equations for well-watered, full cover winter wheat and sorghum and found that the PM formula performed best. Because it is widely used in agricultural and environmental research; and because it has been presented by ASCE (Jensen et al., 1990) and FAO (Allen et al., 1994ab) as a method of computing estimates of reference crop water use, we will discuss the Penman-Monteith equation, which is

$$LE = -\frac{\Delta(R_n + G) + \rho_a c_p (e_s - e_a)/r_a}{\Delta + \gamma(1 + r_s/r_a)} \qquad [5.51]$$

where LE is latent heat flux, R_n is net radiation, and G is soil heat flux (all in MJ m^{-2} s^{-1}); Δ is the slope of the saturation vapor pressure-temperature curve (kPa °C^{-1}), ρ_a is air density (kg m^{-3}), c_p is the specific heat of air (kJ kg^{-1} °C^{-1}), e_a is vapor pressure of the air at reference measurement height z, and e_s is the saturated vapor

pressure at a dew point temperature equal to the air temperature at z (kPa), (e_s - e_a) is the vapor pressure deficit, r_a is the aerodynamic resistance (s/m), r_s is the surface (canopy) resistance (s/m), and γ is the psychrometric constant (kPa °C^{-1}). Penman's equation and those derived from it were developed as a means of eliminating canopy temperature from energy balance considerations. Besides measurements of Rn and G, the user must know the vapor pressure of the air, e_a, and air temperature (from which e_s may be calculated) at reference measurement height, z (often 2 m). The values of r_a and r_s may be difficult to obtain. The surface or canopy resistance is known for only a few crops and is dependent on plant height, leaf area, irradiance, and water status of the plants.

Jensen et al. (1990) and Allen et al. (1994ab) presented methods of calculating E for well-watered, full cover grass and alfalfa. The following example, drawn from recent studies at Bushland, Texas, employs those methods. Aerodynamic resistance was estimated for neutral atmospheric conditions from

$$r_a = \frac{\ln\left(\frac{z_m - d}{z_{0m}}\right)\ln\left(\frac{z_H - d}{z_{0H}}\right)}{k^2 U_z} \qquad [5.52]$$

where z_m (m) is the measurement height for wind speed, U_z, (m/s), z_H (m) is measurement height for air temperature and relative humidity, k is 0.41, z_{0m} and z_{0H} are the roughness length parameters for momentum (wind) and sensible heat transport, and d is the zero plane displacement height. The value of r_a calculated from Equation [5.52] will be too high for highly unstable conditions and too low for very stable conditions. Stability corrections should be made to Equation [5.52] for those conditions (see Monteith and Unsworth, 1990, p. 234 for some examples), but were not made for this example.

Surface resistance was calculated from

$$r_s = \frac{r_l}{0.5 LAI} \qquad [5.53]$$

where r_l is the stomatal resistance taken as 100 s/m, and the leaf area index (LAI) was taken as

$$LAI = 5.5 + 1.5\ln(h_C) \qquad [5.54]$$

where the crop height, hc, was taken as 0.12 cm for grass, and 0.5 m for alfalfa.

The zero plane displacement height, d, was calculated as:

$$d = \frac{2}{3} h_c \qquad [5.55]$$

The roughness length for momentum, z_{0m}, was calculated as:

$$z_{0m} = 0.123\ h_C \qquad [5.56]$$

and the roughness length for sensible heat transport was:

$$z_{0H} = 0.1\ z_{0m} \qquad [5.57]$$

Net radiation was calculated as shown in section 5.1.1.5. All calculations were on a half-hourly basis. For well-watered mixed fescue grass in 1996 the Penman-Monteith (PM) equation underestimated ET, as measured by a weighing lysimeter, at ET rates exceeding 4 mm per day (Fig. 5.25), even though Rn and G were well-estimated. The underestimation of ET was due to systematic error in the surface and/or

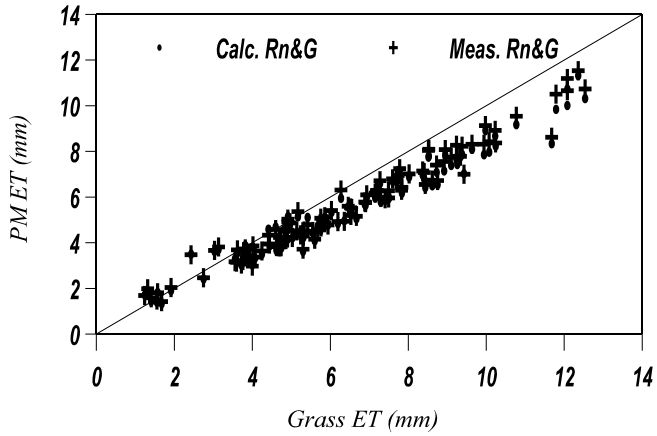

Fig. 5.25. Daily Penman-Monteith estimates of ET using both measured and estimated values of Rn and G were not significantly different from each other for well-watered, full-cover mixed fescue grown at Bushland, Texas in 1996. Both PM ET values were less than values measured by a weighing lysimeter for values above 4 mm d^{-1}

aerodynamic resistances. For well-watered, full-cover alfalfa in 1996 the PM estimates of ET were close to values measured with a weighing lysimeter (Fig. 5.26). Because Rn and G were well-estimated, it is presumed that r_a and r_s were predicted well also. Examination of diurnal dynamics showed that the PM method was capable of closely reproducing those dynamics.

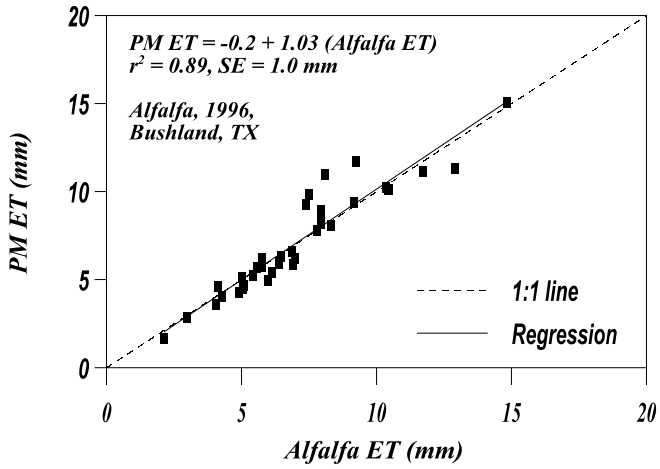

Fig. 5.26. Daily Penman-Monteith estimates of ET using both measured and estimated values of Rn and G were not significantly different from each other for well-watered, full-cover mixed fescue grown at Bushland, Texas in 1996. Both PM ET values were less than values measured by a weighing lysimeter for values above 4 mm d^{-1}

Although important as a research model, the PM method is not much used for direct prediction of LE due to the difficulty of knowing r_a and r_s. However, it is commonly used to predict a theoretical reference evapotranspiration, ET_r, for use in irrigation scheduling (Allen et al., 1994ab). In this application crop water use or ET is predicted from daily values of ET_r and a dimensionless crop coefficient (K_c), which is dependent on the crop variety and time since planting or growing degree days.

$$ET = K_c ET_r \quad [5.58]$$

The crop coefficients are determined from experiments that measure daily crop water use and ET_r and compute

$$K_c = ET/ET_r \quad [5.59]$$

Many details on this methodology are found in Jensen et al. (1990).

Example 5.3: The Penman Approximation - Then and Now.

At the time that Penman (1948), Monteith (1965), and van Bavel (1966) developed their equations for LE, it was very difficult to measure surface temperature of water or plant canopies. All of these equations are called combination equations because they derive from the combination of the energy balance terms given in Equation [5.1] with heat and mass transfer mechanisms. The transfer mechanisms are usually stated as flux equations in terms of resistance(s) or conductance(s) and a gradient of temperature or vapor pressure from the surface to the atmosphere. Penman (1948) restated Equation [5.1] for a wet surface, and substituted transport mechanisms for LE and H to give a combination equation

$$LE = f(u)(e_z - e_o^*) = - [Rn + G + \gamma f(u)(T_z - T_o)] \quad [5.51a]$$

where f(u) is a wind speed dependent conductance or transport coefficient, γ is the psychrometric constant ($c_pP/(0.622\ L)$), e_o^* is the saturation vapor pressure at the surface temperature, e_z is the air vapor pressure at measurement height z, T_z is the air temperature at measurement height, T_o is the surface temperature, and the transport mechanism for H is analogous to Equation [5.73]. The equation can use e_o^* because it is assumed that the surface is "wet", i.e., a free water surface or the canopy of a crop that is full-cover and well supplied with water and thus freely transpiring. Because surface temperature was difficult to measure, Penman (1948) introduced an approximation for (T_o - T_z) that is derived from the slope of the saturation vapor pressure vs. temperature curve, which is (Fig. 5B.2)

$$\Delta = (e_o^* - e_z^*)/(T_o - T_z) \quad [5.51b]$$

From Equation [5.51b] and Fig. 5B.2, we see that

$$e_o^* - e_z = e_z^* - e_z + \Delta(T_o - T_z) \quad [5.51c]$$

Rearranging to find (T_z - T_o) and substituting into Equation [5.51a] gives

$$f(u)(e_z - e_o^*) = -[Rn + G + (\gamma/\Delta)f(u)(e_z - e_o^* + e_z^* - e_z)] \quad [5.51d]$$

or

$$f(u)(e_z - e_o^*) = -[Rn + G + (\gamma/\Delta)f(u)(e_z - e_o^*) + (\gamma/\Delta)f(u)(e_z^* - e_z)] \quad [5.51e]$$

both sides of which hold the identity for LE = $f(u)(e_z - e_o^*)$. Rearranging gives

$$LE = -[\Delta(Rn + G) + \gamma f(u)(e_z^* - e_z)]/(\Delta + \gamma) \qquad [5.51f]$$

which is the Penman equation and is analogous to Equation [5.51]. Rather than use wind functions of the transport coefficient, Monteith recognized the importance of surface resistance and derived the equation in terms of the aerodynamic and surface resistances shown in Equation [5.51].

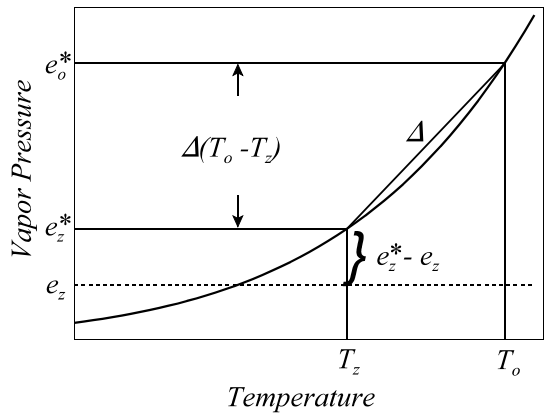

Fig. 5B.2. Quantities used in the derivation of Penman's (1948) combination equation.

Although there is much evidence that the Penman equation and Equation [5.51] are useful for estimating LE from free water and from well-watered, full-cover crops, the results have been disappointing for transfer of wind functions and r_s and r_a formulations between different regions and crops. Some facts about the underlying assumptions should lend insight. First, the value of Δ is usually evaluated at T_z. In humid climes, there may be little difference between canopy and air temperatures, particularly if skies are often overcast. But, in more arid regions the canopy temperature of a freely transpiring crop may be several degrees cooler than air temperature, causing Δ to be overestimated - more so at the hottest part of the day than near sunrise and sunset. Second, the net radiation and soil heat fluxes are modified by the quotient $(1 + \gamma/\Delta)$. This is fundamentally incorrect. The value of γ/Δ ranges from 0.80 at 10°C to 0.17 at 40°C; so the modification of Rn and G is not small, and will change with air temperature over the course of a day. Third, the surrogate in the Penman equation for sensible heat flux is parameterized by vapor pressure terms defined at the same height. Thus, unlike real sensible heat flux, the quantity $\gamma f(u)(e_z^* - e_z)$ can never reverse sign (necessarily, $e_z^* \geq e_z$). Also, over the range from 10 to 40°C, the value of γ varies from 65.5 to 67.5 Pa K^{-1}, while the value of Δ varies from 85 to 402 Pa K^{-1}. To the extent that γ is constant, the division of the vapor pressure deficit by $(\Delta + \gamma)$ causes the surrogate term to vary as H would vary. To the extent that the sum $(\Delta + \gamma)$ varies from Δ, and to the extent that e_z^* differs from e_o^*, the surrogate differs in value from H.

In Equation [5.51], the sum of Rn and G is further modified by the surface and aerodynamic resistances to mass and heat transfer, even though those resistances have negligible effect on the fundamental mechanisms affecting either quantity. (The effect of r_s and r_a on canopy surface temperature has a negligible effect on Rn). These facts have much to do with the difficulties encountered in determining appropriate values of r_a and r_s, and in transferring these values from one

region to another. Also, the fact that wind functions for the Penman equation have been determined to be different for different climates is certainly related to the approximations used in the derivation of the Penman and related equations.

Problem 5.1. Examining the Penman-Monteith Equation

Take the heat capacity of air to be 1010 J kg^{-1} K^{-1}, and air pressure to be 10^5 Pa. Use Equation [5.45] to evaluate L for a range of air temperatures from -10 to 45°C, and evaluate γ for the same range. Take the derivative of Equation [5.34] with respect to temperature and evaluate Δ and γ/Δ for the same range. Would you expect crop coefficients, developed using a Penman-Monteith equation for reference ET in a humid area, to be transferrable to an arid area? Is the wind function in Equation [5.51f] equivalent to a transfer coefficient for sensible heat flux or is it for latent heat flux? How about the surface and aerodynamic resistances in Equation [5.51] - are they for latent heat flux or for sensible heat flux, or perhaps for both? There is much evidence that the transfer coefficients for sensible and latent heat fluxes are not identical, particularly under advective and highly stable conditions. How might this impact the interpretation of data from regions with widely different weather patterns?

At the time that the combination equations were being developed, the instrumentation for measuring net radiation was crude but, compared with that for measuring surface temperature, effective. In the 1960s, the development of infrared radiometers allowed the first radiometric measurements of surface temperature on a large scale, leading to much research on the use of surface temperatures to solve for H using forms of Equation [5.73], and thus to estimate LE from Equation [5.1] (Jackson, 1988). McNaughton (1988) pointed out problems with this method that persist to this day. They include the fact that radiometric surface temperature often differs from aerodynamic surface temperature (the surface temperature that works in Equation [5.73]), the difficulty of evaluating r_a in Equation [5.73] for many surfaces (e.g., partial or mixed canopies), and the spatial heterogeneity of surfaces that leads to spatial heterogeneity of air temperature. However, the continued development of infrared thermometers has led to easy and reliable surface temperature measurement with solid state devices such as the thermocouple infrared thermometer (e.g., the model IRt/c from Exergen, Inc.). Meanwhile, the technology for net radiation measurements has improved, but calibration standards do not exist and it is still common to find differences of 10% or more between competing instruments. Just as the lack of adequate instrumentation for measurement of surface temperature affected the development of theory and practice since 1948, the shift in instrumentation capabilities should affect much of the experimental physics and development of theory and practice for calculation of surface energy and water balances in the next 50 years.

5.2.2.6 Bare Soil Evaporation Estimates

Fox (1968) and later Ben-Asher et al. (1983) and Evett et al. (1994) described an LE prediction method based on subtracting the energy balance equations (Equation [5.1]) written for a dry and a drying soil. Because LE is zero for a dry soil this gives an expression for LE from the drying soil in terms of the other energy balance terms. The method requires a column of dry soil embedded in the field of drying soil; and measurements of the surface temperatures of the dry soil and of the drying field soil. The surface temperature difference between the dry and drying soils explains most of E, but prediction accuracy is only moderately good (r^2 = 0.82 for daily predictions, Evett et al., 1994). Evett et al. (1994) showed that the aerodynamic resistance over the dry soil surface was reduced, probably by buoyancy of air heated over the relatively hot surface; and that the resistance was relatively independent of wind speed. They also showed that consideration of the soil albedo change with drying could improve the E estimates. Although the method shows promise it does not provide an estimate of surface soil water content that would be needed to calculate the albedo change.

When the soil is wet the evaporative flux can be estimated using the Penman or Penman-Monteith equations with surface resistance set to an appropriate low value (Howell et al., 1993). This wet period is the energy-limited stage of evaporation. As the soil dries, E becomes limited by soil properties. Van Bavel and Hillel (1976) addressed this using a finite difference model of soil water and heat flux that later was developed into the CONSERVB model of evaporation from bare soil. This model described one-dimensional soil water movement with Darcy's law, including the dependence of hydraulic conductivity, K (m s^{-1}), on soil water potential, h (m); and the soil water retention function, $\theta_v(h)$. The surface energy balance was solved implicitly for surface temperature (T), resulting in calculated values of E, H, Rn, and G at each time step. The value of E was used as the upper boundary condition for soil water flux at the next time step. The elements of CONSERVB were included in the ENWATBAL model by Lascano et al. (1987); and the latter model was upgraded to model albedo changes dependent on surface soil water content by Evett and Lascano (1993). Although CONSERVB was not validated against directly measured E; the 1993 version of ENWATBAL was shown to more accurately predict E than either the Penman or Penman-Monteith equations (Howell et al., 1993).

5.2.3 Soil Heat Flux

Soil heat flux is discussed in detail in chapter 9. Briefly, heat conduction in one dimension is described by a diffusion equation:

$$C\frac{\partial T}{\partial t} = \lambda\frac{\partial}{\partial z}\left[\frac{\partial T}{\partial z}\right] \qquad [5.60]$$

where the volumetric heat capacity, C (J m^{-3} K^{-1}), and the thermal conductivity, λ (J s^{-1} m^{-1} K^{-1}), are assumed constant in space; and vertical distance is denoted by z, time by t, and temperature by T.

The one dimensional soil heat flux, G, for a homogeneous medium is described by:

$$G = -\lambda\frac{\partial T}{\partial z} \qquad [5.61]$$

The thermal conductivity is a single-valued function of water content and is related to the thermal diffusivity, D_T (m^2 s^{-1}), by:

$$\lambda = D_T C \qquad [5.62]$$

where the volumetric heat capacity, C (J m^{-3} K^{-1}), can be calculated with reasonable accuracy from the volumetric water content, θ_v (m^3 m^{-3}), and the soil bulk density, ρ_b (Mg m^{-3}), by:

$$C = \frac{2.0\times10^6\rho_b}{2.65} + 4.2\times10^6\theta_v + 2.5\times10^6 f_o \qquad [5.63]$$

for a soil with a volume fraction, f_o, of organic matter (Hillel, 1980).

Table 5.6 lists thermal conductivities at 'wet' and 'dry' points for several soils. For coarse soils the thermal conductivity vs. water content curve is S-shaped (see for example, Campbell et al., 1994), with a rapid rise at water contents corresponding to about 33 kPa soil water tension (about 'field capacity'). For fine soils the relationship is more linear; and the thermal conductivity between dry and wet conditions in Table

5.6 can be linearly interpolated from the values given, with reasonably small errors. But for water contents below the 'dry' value the thermal conductivity should be taken as the value corresponding to the 'dry' state.

Table 5.6 Thermal conductivity, λ, of some soil materials.

Soil	Dry θ_v	λ W m^{-1} K^{-1}	Wet θ_v	λ W m^{-1} K^{-1}	ρ_b Mg m^{-3}	Source
Fairbanks sand	0.003	0.33	0.18	2.08	1.71	1
quartz sand	0.00	0.25	0.40	2.51	1.51	1
sand	0.02	0.9	0.38	2.25	1.60	2
sand	0.00	0.27	0.38	1.77	1.64	3
sand	0.003	0.32	0.38	2.84	1.66	4
gravelly coarse sand (pumice)	0.02	0.13	0.40	0.52	0.76	5
medium and coarse gravel (pumice)	0.01	0.09	0.43	0.39	0.44	5
loamy sand	0.01	0.25	0.40	1.59	1.69	6
loam	0.01	0.20	0.60	1.05	1.18	6
Avondale loam	0.08	0.46	0.23	0.88	1.35-1.45	7
Avondale loam	0.03	0.31	0.30	1.20	1.40	9
silt loam	0.09	0.40	0.50	1.0	1.25	2
Yolo silt loam	0.14	0.49	0.34	1.13	1.25	8
Muir silty clay loam	0.03	0.30	0.30	0.90	1.25	9
silty clay loam	0.01	0.20	0.59	1.09	1.16	6
Pullman silty clay loam	0.07	0.16	0.29	0.89	1.3	10
Healy clay	0.04	0.30	0.30	0.91	1.34	1
Fairbanks peat	0.03	0.06	0.61	0.37	0.34	1
forest litter	0.02	0.10	0.55	0.40	0.21	2

1: de Vries, 1963; 2: Riha et al., 1980; 3: Watts et al., 1990; 4: Howell and Tolk, 1990; 5: Cochran et al., 1967; 6: Sepaskhah and Boerma, 1979; 7: Kimball et al., 1976; 8: Wierenga et al., 1969; 9: Asrar and Kanemasu, 1983; 10: Evett, 1994.

De Vries (1963) developed a method of estimating soil thermal conductivity from soil texture, bulk density, and water content. The method, while including most important soil properties affecting conductivity, is limited in that it requires knowledge of parameters called shape factors that describe how the soil particles are packed together. The shape factors are specific to a given soil and perhaps pedon and must be measured. They are, in effect, fitting parameters (e.g. see Kimball et al., 1976). De Vries' method tends to over-estimate thermal conductivity at water contents above about 0.15 (Asrar and Kanemasu, 1983; Evett, 1994). Campbell et al. (1994) developed modifications of de Vries' theory that allowed them to match measured values well. They showed that, as temperature increased, the thermal conductivity vs. water content

curve assumed a pronounced S-shape for the 8 soils in their study; with the curve deviating from monotonicity at temperatures above 50°C.

Horton et al. (1983) developed a measurement method for D_T based on harmonic analysis. The method entailed fitting a Fourier series to the diurnal soil temperature measured at 1-h intervals at 0.01-m depth followed by the prediction of temperatures at a depth, z (0.1 m), based on the Fourier series solution to the one-dimensional heat flux problem using an assumed value of D_T. The value of D_T was changed in an iterative fashion until the best fit between predicted and measured temperatures at z was obtained. The best fit was considered to occur when a minimum in the sum of squared differences between predicted and measured temperatures was found (i.e., minimum sum of squared error, SSE). Poor fits with this and earlier methods are often due to the fact that field soils usually exhibit increasing water content with depth and changing water content with time while the method assumes a homogeneous soil. Costello and Braud (1989) used the same Fourier series solution and a nonlinear regression method, with diffusivity as a parameter to be fitted, for fitting the solution to temperatures measured at depths of 0.025, 0.15 and 0.3 m.

Neither Horton et al. (1983) nor Costello and Braud (1989) addressed the dependency of diffusivity on water content or differences in water content between the different depths. Other papers have dealt with thermal diffusivity in nonuniform soils but did not result in functional relationships between thermal properties and water content, probably due to a paucity of depth-dependent soil water content data (Nasser and Horton, 1989, 1990). Soil water content often changes quickly with depth, time, and horizontal distance. Moreover, diffusivity is not a single valued function of soil water content and so is difficult to directly use in modeling. The ability of time domain reflectometry (TDR) to measure water contents in layers as thin as 0.02 m (Alsanabani, 1991; Baker and Lascano, 1989) provided the basis for design of a system that simultaneously measures water contents and temperatures at several depths. Evett (1994) used measurements of soil temperature at several depths (e.g. 2, 4, 6, 8... cm), coupled with TDR measurements of soil water content at the same depths, to find a relationship between thermal conductivity and water content in a field soil. He used the minimum SSE method of Horton to find the thermal diffusivity for each soil layer between vertically adjacent measurements of water content and temperature. The water content for this layer was used to calculate C and thus λ corresponding to that water content. A function of λ vs. θ_v was developed by regression analysis on the λ and θ_v data (Fig. 5.27). Because both C and λ were known for each layer this method also gave the soil heat flux.

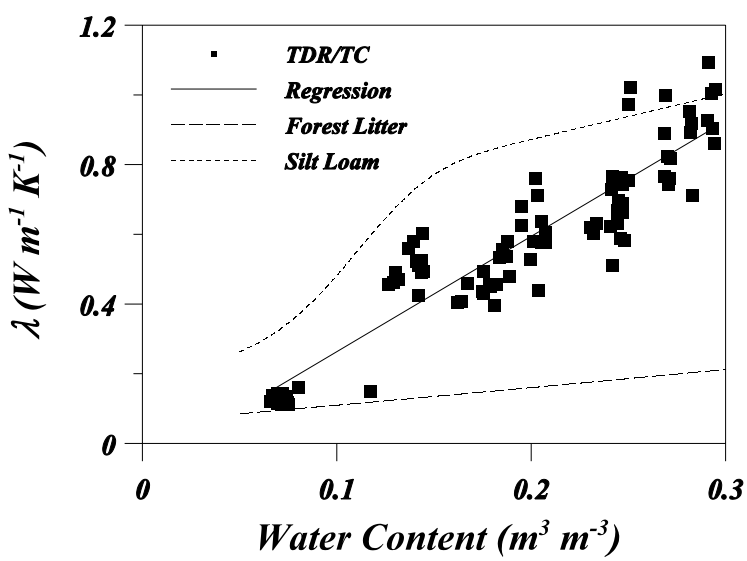

Fig. 5.27 Thermal conductivity of Pullman silty clay loam, determined from TDR probe and thermocouple arrays, compared functions from Campbell (1985) for forest litter and silt loam

Single probe heat pulse methods have been developed to measure thermal diffusivity; and a dual probe heat pulse method (Campbell et al., 1991) can measure the thermal diffusivity, D_T, as well as λ and C (Kluitenberg et al., 1995). Noborio et al. (1996) demonstrated a modified trifilar (three-rod) TDR probe that measured θ_v by TDR, and λ by the dual probe heat pulse method. Their measured λ compared well with values calculated from de Vries (1963) theory.

Soil heat flux is commonly measured using heat flux plates (Table 5.1). These are thermopiles that measure the temperature gradient across the plate, and, knowing the conductivity of the plate, allow calculation of the heat flux from Equation [5.61]. Heat flux plates are impermeable and block water movement. Because of this the plates should be installed a minimum of 5 cm below the soil surface so that the soil above the plate does not dry out or wet up appreciably more than the surrounding soil. Typical installation depths are 5 cm or 10 cm. Even at these shallow depths the heat flux is greatly reduced from its value at the soil surface; and corrections must be applied to compute surface heat flux. The most common correction involves measuring the temperature and water content of the soil at midlayer depths, z_j, in N layers (j to N) between the plate and surface; and applying the combination equation over some time period, P, defined by beginning and ending times t_i and t_{i+1}

$$G = G_z + \frac{\sum_{j=1}^{N} \left(T_{zj_i+1} - T_{zj_i} \right) \Delta z_j C_{zj}}{t_{i+1} - t_i} \qquad [5.64]$$

where G is the surface heat flux during P; G_z is the flux at depth z; the T_{zj} are temperatures at the N depths, z_j, at times t_i and t_{i+1}; Δz_j is the depth of the layer with midpoint z_j; and where the volumetric heat capacities, C_{zj}, at depths z_j are calculated from Equation [5.63], re-written as

$$C_{zj} = \frac{2.0x10^6 \rho_{bzj}}{2.65} + 4.2 \times 10^6 \theta_{vzj} + 2.5 \times 10^6 f_{ozj} \qquad [5.65]$$

where θ_{vzj}, ρ_{bzj}, and f_{ozj} are the water contents, soil bulk densities, and volume fractions of organic matter, respectively, at depths z_j. The estimate of G is not much changed by the exact form of the combination equation as shown by data from Bushland, Texas for four forms of Equation [5.64] (Fig. 5.28). For situations where water content and temperature change rapidly with depth, or bulk density or f_o change rapidly with depth, the multiple layer approach will work better.

The four methods of combining temperature and water content data to correct heat flux for bare soil data collected at Bushland, Texas in 1992 (Fig. 5.28) used the following measurements. Temperatures were measured at 2- and 4-cm depths (2 replicates) with thermocouples, T_2 and T_4; at the surface with a single infrared thermometer, T_0; and as a mean temperature of the surface to 5-cm depth soil layer using thermocouples wired in parallel and buried (4 replicates) at 1- and 4-cm depths, T_{1_4}. Water contents were measured by TDR probes (2 replicates) inserted horizontally at 2- and 4-cm depths, θ_2 and θ_4. Soil heat flux at 5-cm depth, G_5, was measured with heat flux plates (4 replicates). For all methods the product of soil bulk density and heat capacity of soil solids was set to 1.125 MJ m^{-3}. For the first method the surface heat flux, G_0, was

$$G_0 = G_5 + \frac{\left(1.125 + 4.2\theta_w\right) \times 10^6 (0.05) \left(T_{w+1} - T_w\right)}{1800} \qquad [5.66a]$$

where 1800 was the period in s; the weighted water content for the surface to 5-cm depth layer, θ_w, was

$$\theta_w = 3\theta_2/5 + 2\theta_4/5 \qquad [5.66b]$$

the weighted temperature for the surface to 5-cm depth layer, T_w, was

$$T_w = 3T_2/5 + 2T_4/5 \qquad [5.66c]$$

and T_{w+1} was the same, but for the previous measurement.

For the second method, θ_w and the series-wired thermocouple temperature were used

$$G_0 = G_5 + \frac{\left(1.125 + 4.2\theta_W\right) \times 10^6 (0.05)\left(T_{1_4+1} - T_{1_4}\right)}{1800} \qquad [5.67]$$

For the third method, θ_w was used

$$G_0 = G_5 + \frac{\left(1.125 + 4.2\theta_W\right) \times 10^6 (0.05)\left(T_{024+1} - T_{024}\right)}{1800} \qquad [5.68a]$$

but the depth weighted mean, T_{024}, of infrared thermometer temperature and those measured at 2 and 4 cm was used.

$$T_{024} = \frac{\left[\frac{(T_0 + T_2)/2 + T_0}{2}\right]}{5} + \frac{2T_2}{5} + \frac{2T_4}{5} \qquad [5.68b]$$

For the fourth method a modified layer approach was used

$$G_0 = G_5 + \frac{\left(1.125 + 4.2\theta_2\right) \times 10^6 (0.05)\left(T_{02+1} - T_{02}\right)}{1800} + \frac{\left(1.125 + 4.2\theta_4\right) \times 10^6 (0.05)\left(T_{4+1} - T_4\right)}{1800} \qquad [5.69a]$$

where the depth weighted mean temperature in the surface to 3-cm deep layer, T_{02}, was

$$T_{02} = \frac{\left[\frac{(T_0 + T_2)/2 + T_0}{2}\right]}{3} + \frac{2T_2}{3} \qquad [5.69b]$$

All of these methods produced similar values of G_0, but those using a depth-weighted water content tended to overestimate extreme values, probably because the 2-cm water content was lower than that at 4 cm. The weighted mean approach for both water content and temperature, with surface temperature included, (Equation [5.68]) produced generally the largest diurnal swing in G_0. Methods that didn't include the surface temperature, but used the weighted mean approach for both water content and temperature (Equations [5.66] and [5.67]) produced intermediate results. The layer approach (Equation [5.69]), produced the smallest diurnal swing in G_0, despite using the surface temperature, and is probably the most accurate approach. All methods corrected both the amplitude and the phase of the diurnal cycle of G_0 appropriately.

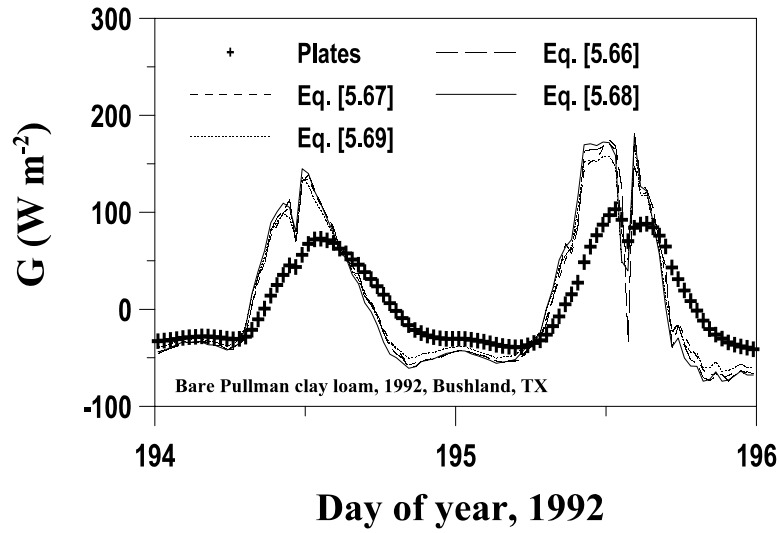

Fig. 5.28 Four methods of correcting heat flux, measured with plates at 5-cm depth, to surface heat flux

Convective heat flux can play an important role in soil heating or cooling. This is the heat transported by moving air or water, the latter denoted in Fig. 5.1 by G_{Jw} for heat transported by infiltrating water. Because of the low heat capacity of air the convective heat flux due to air movement is usually small, but convective heat flux due to infiltration of water can be much larger than that due to diffusion on a diurnal basis. For example, irrigation with 5 cm of water at 15°C on a soil at 25°C with an initial water content of 0.1 m^3 m^{-3} and a bulk density of 1.48 would immediately lower the temperature of the 11.6 cm deep wetted layer to 20 °C (assuming negligible heat of wetting, the soil brought to saturation, and a heat capacity of 1.54 MJ m^{-3} K^{-1}). The heat of wetting is usually not large enough to be important in heat balance calculations. It can be large for clays with large surface area if they are extremely dry, ranging from 40 J g^{-1} for kaolinitic clays to 125 J g^{-1} for allophanic clays (Iwata et al., 1988). But, it decreases quickly as the initial water content of the soil increases, and is not likely to be important for the normal range of field water contents.

Example 5.4: Estimating Soil Thermal Conductivity - The Sine Wave Approach.

The complicated methods of measuring thermal diffusivity and conductivity mentioned here use computer programs and nonlinear regression fitting of multi-term sine series in order to handle diurnal temperature waves that differ from simple sinusoidal waves, as well as to incorporate measurements of soil water content that vary with depth. However, rough estimates of the thermal parameters may be made from phase differences and amplitude differences observed for temperatures measured at only two depths, with the application of simplifying assumptions of homogeneous water content and soil properties, and a simple sinusoidal diurnal temperature wave describing the temperature T at depth z and time t

$$T(z,t) = \overline{T} + A_z \sin[\omega t + \phi(z)] \qquad [5.60a]$$

where $\overline{T}$ is the mean temperature (i.e., the mean of maximum and minimum for a sine wave), A_z is the amplitude of the wave (i.e., the difference between maximum and minimum temperatures), ω is

$2\pi/\tau$ where τ is the period (e.g., 24 h), and $\phi(z)$ is the phase angle at depth z (difference in time between the occurrence of the maxima or minima at depth 0 and depth z). Equation [5.60] can be solved using the above equation for T(z, t) yielding

$$T(z,t) = \overline{T} + A_0 \sin[\omega t - z/d] / e^{z/d} \qquad [5.60b]$$

where A_0 is the amplitude at depth zero, and d is called the damping depth and is a function of the thermal conductivity and volumetric heat capacity

$$d = (2\lambda/C\omega)^{1/2} \qquad [5.60c]$$

When z equals d, the amplitude is 1/e = 0.37 of the amplitude at depth zero. Writing Equation [5.60b] for two depths, z_1 and z_2, and solving for λ/C gives

$$\lambda / C = \frac{\pi(z_2 - z_1)^2}{\tau[2.3\log(A_1 / A_2)]^2} \qquad [5.60d]$$

Figure 5B.3 shows measured diurnal temperature waves for several depths in a Pullman clay loam on two different days. Table 5B.1 gives the mean water content as measured by time domain reflectometry for each depth. Also shown are the thermal conductivities obtained by fitting a sine series to each depth and evaluating the thermal conductivity of the layer between depths by using the coefficients of the sine series in a sine series solution to T(t) at the next depth and then performing a nonlinear fit of that solution to obtain the thermal conductivity.

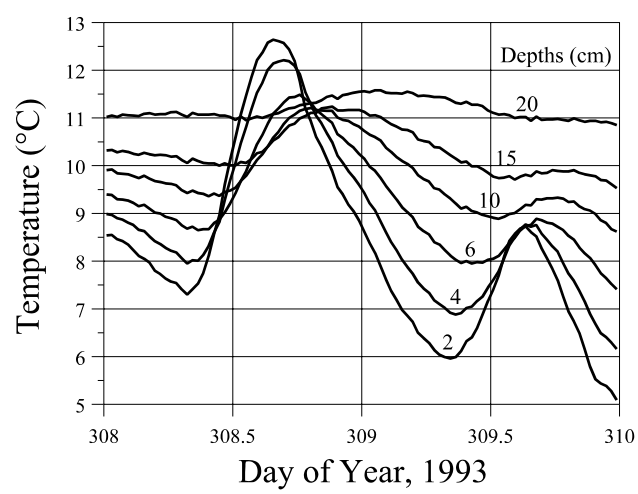

Fig. 5B.3. Temperatures at six depths in a Pullman clay loam for two days in 1993.

Problem 5.2. Estimating Soil Thermal Conductivity

Using Equation [5.60d], measure the amplitudes of each vertically adjacent pair of diurnal waves in Fig. 5B.3 and solve for the thermal conductivity of the layer between. Calculate C from Equation [5.63] assuming zero organic matter, a bulk density of 1.4 Mg m^{-3}, and using the mean water content for the layer. Repeat the calculations assuming that you knew only the mean water content for the surface to 30-cm depth (0.23 m^3 m^{-3}). Why are your values for λ different than those from the nonlinear fit? How often do you think that the assumption of soil homogeneity that allows Equations [5.60] to be written is true? On these cool fall days, the mean soil temperature increased with depth; but on day 308, there was not much difference between the means at 2 and at 20 cm. However, on day 309 a cool front caused the surface temperature to decline sharply, and the mean temperature was several degrees cooler at 2 cm than at 20 cm. Which set of thermal conductivities in Table 5B.1 are more likely to be correct, those for day 308 or those for day 309? Explain why the thermal conductivities estimated by nonlinear fit for day 309 are different than those for day 308 even though the water contents differ at most by 0.01 m^3 m^{-3}. Why is the estimate from Equation [5.60d] for the 15-20 cm layer on day 308 in better agreement with the nonlinear fit estimate than any other?

Table 5B.1. Mean soil water contents, θ (m^3 m^{-3}), and thermal conductivities, λ (J m^{-1} s^{-1} K^{-1}), calculated from a nonlinear fit of a sine series solution to Equation [5.60] for a Pullman clay loam for two days in 1993.

Depth (cm)	θ (m^3 m^{-3})	Amplitude based Eq. 5.60d $\lambda_{\theta=\text{interlayer mean}}$	Amplitude based Eq. 5.60d $\lambda_{\theta=0.23}$	Nonlinear fit - sine series soln. λ_{θ}
		Day 308		
2	0.09			
		0.176	0.232	0.138
4	0.14			
		0.518	0.577	0.485
6	0.22			
		0.740	0.717	0.709
10	0.27			
		1.128	1.003	1.221
15	0.31			
		1.295	1.151	1.271
20	0.27			
		Day 309		
2	0.08			
		0.082	0.111	0.117
4	0.13			
		2.273	2.566	0.363
6	0.22			
		3.850	3.772	0.596
10	0.26			
		3.008	2.700	0.916
15	0.31			
		2.006	1.784	1.098
20	0.27			

Example 5.5: Bernoulli, Soil Air, and Convective Heat Flux.

Convective heat flux due to air movement into and out of soil surfaces is commonly ignored in energy balance considerations. Most people do not see any reason for air to move into or out of soil other than changing atmospheric air pressure. However, there are other forces at play that may significantly increase air flow into or out of soil surfaces. Consider Bernoulli's theorem,

$$\frac{v_1^2}{2g} + \frac{p_1}{\rho g} + z_1 = \frac{v_2^2}{2g} + \frac{p_2}{\rho g} + z_2 \qquad [5.69c]$$

which is an equation of conservation of energy where v_1 and v_2 are fluid velocities at two points, p_1 and p_2 are the respective fluid pressures, ρ is the density of air and g is the acceleration due to gravity, and z_1 and z_2 are the elevations of the two points. Taking air as the fluid and placing point 1 in the soil and point 2 in the atmosphere directly above the soil, we see that $v_1 \approx 0$, and $v_2 \geq 0$ so that the equation may be rewritten as

$$p_1 - p_2 = \frac{\rho v_2^2}{2} + (z_2 - z_1)\rho g \qquad [5.69d]$$

That is, the pressure differential from soil to air is equal only to the elevation difference multiplied by ρg when wind speed is zero, and increases above that value as the square of wind speed. During sustained winds across flat surfaces, there is a sustained pressure gradient driving air movement from soil to air. For air movement over non-planar surfaces, the situation is complicated by other aerodynamic effects such as drag, which may increase or decrease the pressure gradient at various places over the surface.

Problem 5.3. Bernoulli's Equation, Soil Air Movement, and Convective Heat Flux.

Now, consider that soil air is usually at nearly 100% relative humidity. For a sustained wind of 10 m/s over a flat surface, calculate the total potential gradient for air movement from the soil to the atmosphere 2 m above the surface, and calculate the convective heat flux due to air movement out of the soil if the soil temperature is 35°C, the air temperature is 15°C, and its relative humidity is 25%. Assume that air is incompressible and that Darcy's law applies (section 8.1.6.1), and estimate conductivity from section 8.2.2 and a water saturation of 0.1 (or see section 8.4.1). Is this magnitude of heat flux likely to continue for extended periods of time (explain why or why not)? How does it compare with the magnitudes of other energy fluxes described in this chapter? Could this mechanism enhance evaporative loss from the soil? What might happen if the surface were hilly? How would the energy flux change if the surface were covered with a 0.3-m tall wheat stubble? Would depth to the water table have an effect on the outcome - 1) if the depth were 1 m, 2) if the depth were 100 m? Why do ice caves form in porous rock formations that are otherwise well above the freezing point of water?

5.2.4 Sensible Heat Flux (H)

Sensible heat flux is the transfer of heat away from or to the surface by conduction or convection. Because air is not a very good conductor of heat most sensible heat flux is by convection (movement) of air. This occurs in eddies of different scales depending on the turbulence of the atmosphere near the surface. Turbulence is influenced by the aerodynamic roughness of the surface, the wind speed, and the temperature differential between the surface and the air. Perhaps the most common method of evaluating sensible heat flux is to measure the other terms in Equation [5.1] as accurately as possible and then set H equal to the residual

$$H = - Rn - G - LE \qquad [5.70]$$

Of course this approach lumps all the errors in the other terms into H. More importantly it does not allow for a check on the accuracy of the energy balance. By definition, if H is defined by Equation [5.70] then Equation [5.1] will sum to zero. Only an independent measure of H can provide a check sum for Equation [5.1].

As noted in section 5.2.2.2, eddy correlation is a direct method of measuring H

$$H = \overline{\rho_a} c_p \overline{w'T'} \qquad [5.71]$$

where the overbars denote short time averages of air density, ρ_a, vertical wind speed, w′, and air temperature, T′, measured at some height within the constant flux layer.

The Bowen ratio method can be applied to sensible heat flux as well as to latent heat flux as outlined in section 5.2.2.3. For sensible heat flux the Bowen ratio is (following Rosenberg et al., 1983, p. 256)

$$H = \frac{-(Rn + G)}{\left(1 + \frac{1}{\beta}\right)} \qquad [5.72]$$

The considerations of fetch, measurement height, equipment, etc. mentioned in section 5.1.2 for Bowen ratio and eddy correlation measurements apply as well to sensible heat flux measurements made with these methods.

Though obviously a dynamic and complex process, sensible heat flux, H (W m^{-2}), is sometimes estimated using a straightforward resistance equation

$$H = \frac{\rho c_p (T_z - T_0)}{r_{aH}} \qquad [5.73]$$

where ρ is the density of air ($\rho = 1.291 - 0.00418T_a$, with less than 0.005 kg m^{-3} error in the -5 to 40°C range, T_a in °C), c_p is the heat capacity of air (1.013×10^3 J kg^{-1} K^{-1}), T_z is the air temperature at measurement height, r_{aH} is the aerodynamic resistance to sensible heat flux (s m^{-1}), and T_0 is the temperature of the surface. [For vegetation, the 'surface' for aerodynamic resistance is the height at which the logarithmic wind speed profile, established by measurements of wind speed above the surface, extrapolates to zero. This height is $d + z_{om}$ and is often well below the top of the canopy, typically at 2/3 to 3/4 h. Measurements of surface temperature (with, for instance, an infrared thermometer) may not be the mean temperature at the same height as the aerodynamic 'surface', thus causing some problems with r_{aH} estimation. Also, the roughness length for momentum, z_{om}, may be different from that for sensible heat, z_{oH}]

A general form for r_a is:

$$r_a = \frac{1}{k^2 u_z}\left[\ln\left(\frac{z - d}{z_0}\right)\right]^2 \qquad [5.74]$$

where k is the von Kármán constant = 0.41, z_o is the roughness length (m), z is the reference measurement height (m), u_z is the wind speed (m/s) at a that height. and d is the zero plane displacement height (m). Equation [5.74] only holds for neutral stability conditions. Unstable conditions occur when the temperature (and thus air density) gradient from the surface upwards is such that there is warm air rising through the atmosphere. Stable conditions prevail when the air is much cooler and denser near the surface, thus inhibiting turbulent mixing. Neutral conditions obtain when neither stable nor unstable conditons do.

For bare soil Kreith and Sellers (1975) simplified Equation [5.74] to:

$$r_a = \frac{1}{k^2 u_z}\left[\ln\left(\frac{z}{z_0}\right)\right]^2 \qquad [5.75]$$

where u_z is the wind speed (m/s) at the reference height (z) (m). They found a value of z_o = 0.003 m worked well for smooth bare soil.

For non-neutral conditions a variety of stability corrections have been proposed. See Rosenberg et al. (1983, pp. 140-144) and Monteith and Unsworth (1990, p. 234-238). Because many models of the soil-plant-atmosphere continuum use Equation [5.73] to model H it is important to note that, while stability corrections can improve model predictions of H and surface temperature, the stability corrections are implicit in terms of H. This leads to a requirement for iterative solution of sensible heat flux at each time step in these models.

Knowledge of appropriate values for d and z_0 in the above equations can be hard to come by. Campbell (1977) suggests estimating these from plant height, h, as

$$d = 0.64\ h \qquad [5.76]$$

for densely planted agricultural crops; and

$$z_{0m} = 0.13\ h \qquad [5.77]$$

for the roughness length for momentum for the same condition. Campbell (1977) gives the roughness length parameters for sensible heat, z_{0H}, and vapor transport, z_{0v}, as

$$z_{0H} = z_{0v} = 0.2\ z_{0m} \qquad [5.78]$$

Note that Equation [5.78] differs from Equation [5.57] where Jensen et al. (1990) used $z_{0H} = 0.1\ z_{0m}$. For coniferous forest Jones (1992) gives

$$d = 0.78\ h \qquad [5.79]$$

and

$$z_{0m} = 0.075\ h \qquad [5.80]$$

for these parameters. As wind speeds increase many plants change form and height, with resulting decrease in h, d, and z_{0m}. It is unlikely that the relationships given in Equations [5.76-5.80] hold true for high wind speeds.

5.3 WATER BALANCE EQUATION

The water balance is written for a control volume of unit surface area; and with a vertical dimension that extends from the soil surface to a lower boundary that is usually assigned a depth at or below the bottom of the root zone (Fig. 5.1)

$$0 = \Delta S - P + R - F - E \qquad [5.81]$$

where ΔS is the change in soil water storage in the profile, P is precipitation or irrigation, R is the sum of runoff and runon, F is flux across the lower boundary of the profile, and E is water lost to the atmosphere through evaporation from the soil or plant or gained by dew formation. The value of P is always positive or zero; but values of ΔS, R, F, and E may have either sign. By convention, R is taken to be positive when there is more runoff than runon. Also conventionally, E is often taken to be positive when flux is out of the control volume. Here, in order to be compatible with the energy balance equation, we will break with convention and take E as positive towards the surface of the soil. The equation is often re-arranged to provide values of E when suitable measurements or estimates of the other terms are available; but it can and has been used to estimate runoff, soil water available for plants, and deep percolation losses (flux downward out of the profile). Here, we take F as positive when flux is upward across the lower boundary into the control volume. The term F is used rather than P for deep percolation, both to avoid confusion with precipitation, and to avoid the common misconception that flux is only downward when P is used to indicate deep percolation.

Usually, the values of terms in Equation [5.81] are given as equivalent depths of water per unit area (e.g. mm/m^2). In the case of E the units of kg m^{-2} may be conveniently converted to mm by dividing by 1 kg m^{-2} mm^{-1}, with little loss of accuracy because the density of water in units of kg L^{-1} is not quite unity (One liter = 1000 cm^3 = the volume of a right rectangular prism with sides 1 m, 1 m, and 1 mm.). The change in storage (ΔS) is often determined by measuring soil water content changes by methods that give volumetric water content, θ_v (m^3 m^{-3}). Multiplying the water content by the depth of the layer gives the depth of water stored. In the United States, the term evapotranspiration (ET) is used to represent the sum of evaporative fluxes from the soil and plant. By convention, ET is taken as positive for fluxes from plant or soil surface to the atmosphere. Thus, ET = -E/(1 kg m^{-2} mm^{-1}) and the water balance may be re-arranged as

$$\Delta S = P - R + F - ET \qquad [5.82]$$

This provides a use for the ET term for those who prefer to say evaporation rather than evapotranspiration. Examination of Equation [5.82] will satisfy the reader that soil water storage increases with precipitation, decreases if runoff from precipitation occurs, decreases with increasing ET, and increases with flux upward into the control volume.

5.3.1 Measuring ΔS and ET

Probably the most accurate method of measuring ΔS is the weighing lysimeter (Wright, 1991). Although large weighing lysimeters involve considerable expense, they can give very precise measurements (0.05 mm = 0.05 kg m^{-2}) (Howell et al., 1995). An excellent review of the use of weighing lysimeters is given by Howell et al. (1991). Careful design, installation, and operation will overcome any of the serious problems

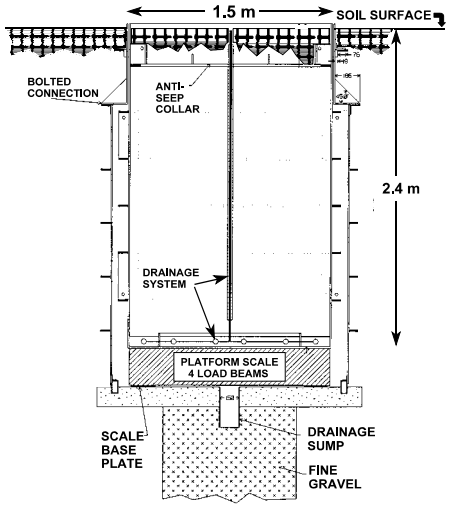

Fig. 5.29 Cross-sectional view of simplified weighing lysimeter installed for grass reference ET measurements at Bushland, TX (Scheider, 1998a)

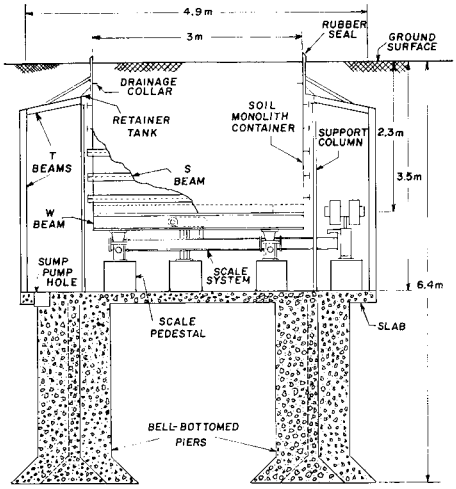

Fig. 5.30 Cross-sectional view of one of the four large weighing lysimeters at Bushland, TX (Schneider, 1998b)

reported with some lysimeters including disturbance of the soil profile (less with monolithic lysimeters), interruption of deep percolation and horizontal flow components, uneven management of lysimeter compared with field soil (Grebet and Cuenca, 1991), and other sources of bias (Ritchie, et al., 1996). Other drawbacks include heat flux distortions caused by highly conductive steel walls (Black et al., 1968; Dugas and Bland, 1991, but minimal for large lysimeters) and high cost, e.g., US$ 65,000 (Lourence and Moore, 1991) and US$ 80,000 (Marek et al., 1988).

Schneider et al. (1996) described simplified monolithic weighing lysimeters (Fig. 5.29) that were considerably less expensive than, and nearly as accurate as, the monolithic weighing lysimeters described by

Marek et al. (1988) (Fig. 5.30). These two designs represent contrasts in mode of operation and each presents some advantages and disadvantages. The design in Fig. 5.30 allows access to all sides and the bottom of the lysimeter for installation or repair of sensors and weighing or drainage systems. The Campbell Scientific, Inc. CR7 data logger that handles all measurements is installed in the underground chamber and typically is subject to only a small diurnal temperature swing of 1°C, reducing temperature induced errors in low level measurements such as load cell transducer bridges and thermocouples. Other equipment installed in the chamber includes a system for time domain reflectometry measurements of soil water content and concurrent measurements of soil temperature, and an automatic vacuum drainage system that continuously monitors drainage rate. The drainage tanks are suspended by load cells from the bottom of the lysimeter tank, allowing measurement of tank mass change without changing the mass of the lysimeter until the tanks are drained (manual but infrequent). The main disadvantages of this design are the shallow soil depth over the ceiling around the periphery of the chamber, and the surface area taken by the entrance hatch. The shallow soil depth can cause uneven plant growth next to the lysimeter, but this problem has been eliminated with the installation of a drip irrigation system to apply additional water to this area. The soil disturbed to install the outer chamber wall appears to have returned to a condition similar to the rest of the field. Access to the lysimeter must be carefully managed to avoid damage to the crop.

Example 5.6: Surface Storage – The Human Contribution.

Surface storage is ignored in the discussion of soil water balance here, but it not only has a large influence on the amount of water infiltrated from a precipitation or irrigation event, but it is one of two factors that are the most amenable to human control both on a small and large scale. The other is infiltration rate, a soil property that may be increased by soil tillage over the short term, and decreased by tillage in the long term, and also may be influenced by no tillage or minimum tillage practices, by tree plantings and ground covers designed to protect the soil surface from slaking and crusting, and many other practices. Many farming efforts are aimed at increasing surface storage through practices like plowing to roughen the soil surface, or furrow diking to create infiltration basins and decrease runoff, to name two. Soil conservation measures such as terraces, contour bunds, etc. are aimed at decreasing runoff or runoff velocity, and thus increasing the opportunity time for infiltration. On the other hand, water harvesting is a practice of increasing runoff by reducing both surface storage and infiltration rate, with the aim of using the runoff water elsewhere. Among the oldest artifacts of human cultivation are water harvesting systems that included the removal of gravel from desert surfaces to improve runoff, terrace systems for guiding and reducing runoff, and in some cases the combined use of both technologies to concentrate water on an area chosen for cultivation. To the extent that such practices influence infiltration, they will affect the timing, magnitude, and spatial patterns of such energy balance terms as sensible and latent heat fluxes, and the convective heat flux accompanying infiltrating water.

Figure 5.29 shows a design that minimizes disturbance to the field during both installation and operation. The monolith was collected a short distance away, and the outer box was installed in a square hole that disturbed only a 15 cm perimeter of soil outside the lysimeter. Because there is no access to the sides or bottom of the lysimeter there is no reason for personnel to visit the lysimeter area except for crop management and the occasional manual drainage accomplished with a vacuum pump and collection bottle. A disadvantage of this design is that continuous drainage rates are not available. The CR7 data logger is located 30 m away in a weather-tight enclosure, and all cables are buried. The location of the CR7 inside the lysimeter chamber in Fig. 5.30 allows a four wire bridge to be used for reading the weighing system load cell. The long cable lengths to the external CR7 used with the lysimeter in Fig. 5.29, and the large diurnal temperature swing to which cables and CR7 are exposed, both cause a six wire bridge to be needed to eliminate errors due to

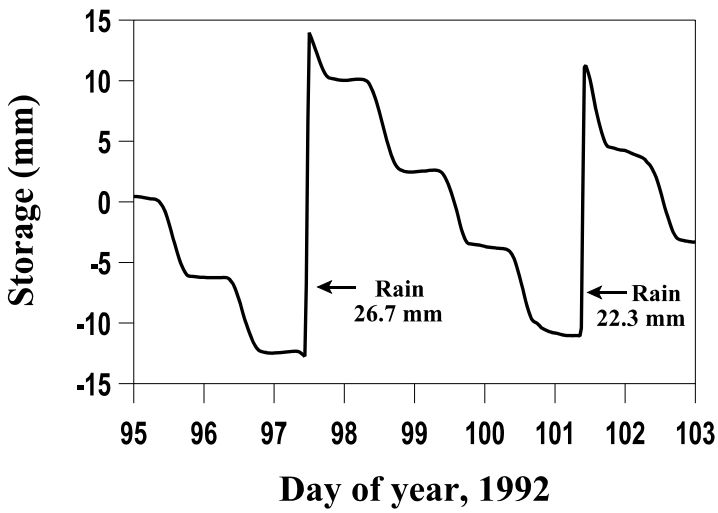

Fig. 5.31 Unadjusted weighing lysimeter storage for winter wheat at Bushland, TX

temperature induced resistance changes when reading the platform scale load cells. Measurement precision with the lever beam scale in Fig. 5.30 is 0.05 mm while that with the platform scale in Fig. 5.29 is 0.1 mm.

Weighing lysimeters measure mass change over a given time, ΔM. If mass is measured in kg then dividing the mass change by the surface area in m^2 of the lysimeter will give the change in water storage, ΔS, of the lysimeter as an equivalent depth of water in mm, with only slight inaccuracy due to the density of water not being quite equal to 1 kg L^{-1}. If only daily ET values are needed then ΔS is computed from the 24 h change in lysimeter mass, usually midnight to midnight. Some averaging of readings around midnight may be needed to smooth out noise. By adding any precipitation or drainage the daily ET is computed. Data from a continuously weighing lysimeter may be presented as a time sequence of mass (or depth of water storage) referenced to an arbitrary zero (Fig. 5.31). Often irrigation or precipitation events will show as obvious increases in storage (Fig. 5.31), and drainage events will show up as decreases in storage. Adjusting the sequential record of storage amount by adding the rainfall or irrigation depth, or the drainage depth, at the time that these occurred, will remove these changes in storage, and is equivalent to the operations defined by the +P and +F in Equation [5.82]; resulting in the monotonically decreasing storage shown in Fig. 5.32. Taking the first derivative of the adjusted storage with respect to time gives the adjusted ΔS rate, and thus ET rate if R and F are zero (Fig. 5.33). In order to compute ET rates on the same time interval as lysimeter mass measurements are made, we must have concurrent measurements of irrigation, precipitation and drainage on the same or a finer recording interval.

Weighing lysimeters are subject to wind loading, more so when the soil surface is bare, as evidenced by Fig. 5.34 In windy regions it may be necessary to smooth the data to remove noise when calculating the ET rate. Gorry (1990), following Savitsky and Golay (1964), described a method for general least squares smoothing that allowed application of different levels of smoothing to both raw data and first derivative. Application of this method to post-processing of data is preferable to real-time smoothing that may eliminate detail in the data. With post-processing we can apply only the amount of smoothing needed to reduce noise to acceptable levels. A computer program to apply Savitsky-Golay smoothing is available (http://www.cprl.ars.usda.gov/programs/).

Microlysimeters are small enough to be installed and removed by hand for weighing daily or more often. They can give good precision but are sensitive to spatial variability. Lascano and Hatfield (1992) showed that 182 microlysimeters were required to measure field average E with precision of 0.1 mm d^{-1} at a 90% confidence level when their soil was wet; but only 39 when dry. This was due to the greater variability of

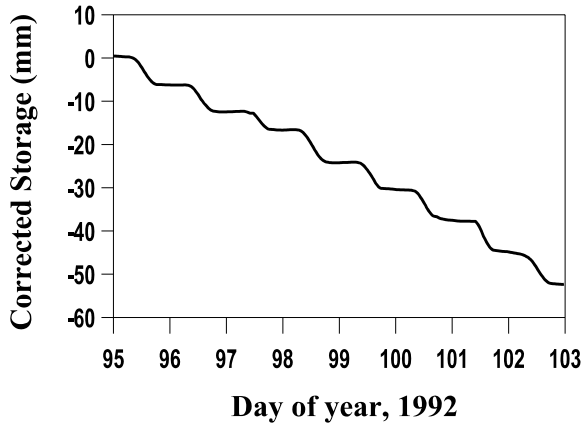

Fig. 5.32. Lysimeter storage values from Fig. 5.31 adjusted by subtracting precipitation amounts

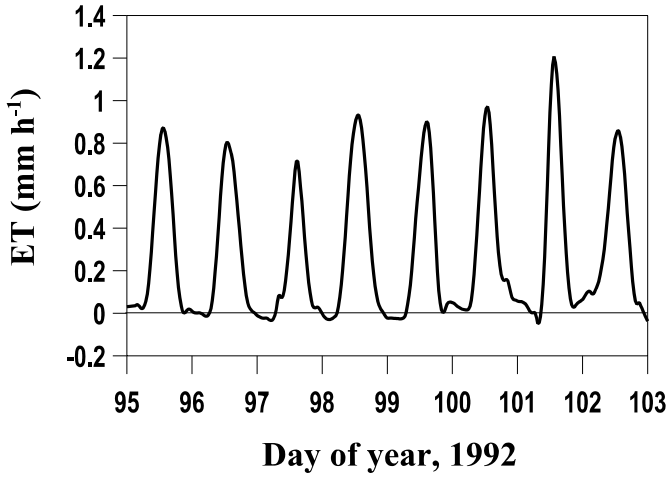

Fig. 5.33. Evapotranspiration rate calculated by taking the negative of the first derivative of adjusted storage from Fig. 5.32. The negative ET rates shown for some nights are caused by dew formation

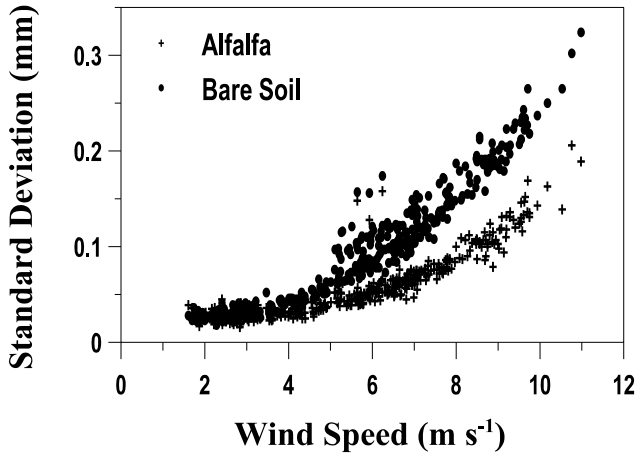

Fig. 5.34. Half-hourly standard deviations of lysimeter storage (mm) as affected by wind speed over contrasting surfaces for days 97-105 at Bushland, TX in 1994

E for wet soil. For a precision of 0.5 mm d^{-1} only 7 microlysimeters were required for any soil wetness. To avoid heat conduction to and from the surface, microlysimeter walls should be made of low thermal conductivity materials such as plastic; and, to avoid trapping heat at the bottom of the microlysimeter, the bottom end cap should be made of a thermally conductive material such as metal (Evett et al., 1995). Plastic pipe makes good microlysimeters. Typical dimensions are 7.6 or 10 cm in diameter, and from 10 cm to 40 cm high. Beveling the bottom end eases insertion into the soil. Typical practice is to insert the microlysimeter vertically until its top is level with the soil surface; then dig it out, or rotate it to shear the soil at the bottom, and pull it out. After capping the bottom with a water-tight seal, it is weighed before re-insertion into the original or a new hole; sometimes lined with a material (e.g. plastic sheet or bag) to prevent sticking of the soil to the microlysimeter outside surface. After a period of time the microlysimeter is re-weighed and the difference in initial and final weights is the evaporative loss. Short microlysimeters should be replaced daily, as the water supply is soon used up to the point that the soil inside the lysimeter is no longer at the same water content as the soil outside. In a study of spatial variability of evaporation from bare soil, Evett et al. (1995) used 30 cm high microlysimeters to avoid daily replacement so that the spatial relationship would not be changed. They showed that for their clay loam soil the 30 cm height was adequate for 9 days. If plant roots are present it is recommended to replace microlysimeters daily to lessen errors associated with root water uptake that occurs elsewhere in the field but not in the microlysimeters.

Alternatives to weighing lysimetry include soil water measurement methods for assessing ΔS for a soil profile of given depth over a given time. In this case the soil volume of interest is unbounded below the surface and F is, strictly speaking, uncontrolled. Measurements of soil water content can give the change in soil water stored in a profile of given depth with good accuracy; and can give good values for E if water flux across the bottom of the profile is known or can be closely estimated. Baker and Spaans (1994) described a microlysimeter with TDR probe installed vertically to measure the water content. Comparison of E calculated from the change in storage closely matched the E measured by weighing the microlysimeter. Young et al. (1997) showed that a single 800 mm long probe installed vertically from the surface could account for 96% of ET from weighing lysimeters irrigated on a 6 d interval; but standard error for the probe was about 4 times larger than that for the lysimeter (0.46 and 0.07 mm, respectively). In a container study with a sorghum plant, Wraith and Baker (1991) showed that a TDR system could measure ET with high resolution and provide measurements of change in storage on a 15 min interval that compared very well with those measured by an electronic scale.

Evett et al. (1993) showed that change in storage in the upper 35 cm of the profile under winter wheat could be accurately tracked with horizontally placed TDR probes, with an average of 88% of daily ΔS occurring in the upper 30 cm. But, E estimates were incorrect (compared with a weighing lysimeter) when flux across the 30 cm boundary occurred. However, combination of the TDR system with neutron probe measurements of deeper soil moisture allowed measurement of E to within 0.7 mm of lysimeter measured E over a 16 d period; five times better than the accuracy achieved using only neutron probe measurements.

Figure 5.35 shows the soil water storage (referenced to arbitrary zero) as measured for winter wheat by weighing lysimeter and two TDR arrays. Each TDR array consisted of seven probes inserted horizontally into the side of a pit and the pit backfilled after wheat planting. Probe depths were 2, 4, 6, 10, 15, 20, and 30 cm, and the probes were read every half hour. Rains on days 101, 104, and 106 can be seen as increases in the storage amount. Changes in storage as measured by the two systems were nearly identical in the seven day period shown (Fig. 5.36); and ET amounts were closely similar (Fig. 5.37).

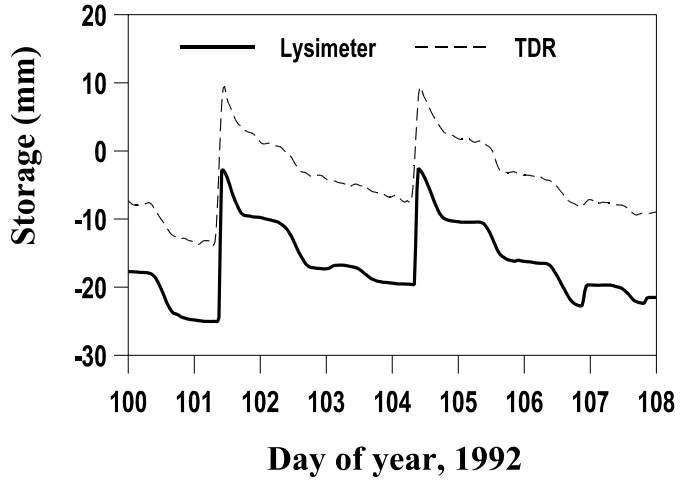

Fig. 5.35. Soil water storage in the upper 35 cm of the soil profile, as measured by two TDR probe arrays, compared with storage in a 2.4-m deep weighing lysimeter. Zero reference is arbitrary. Winter wheat, Bushland, Texas, 1992

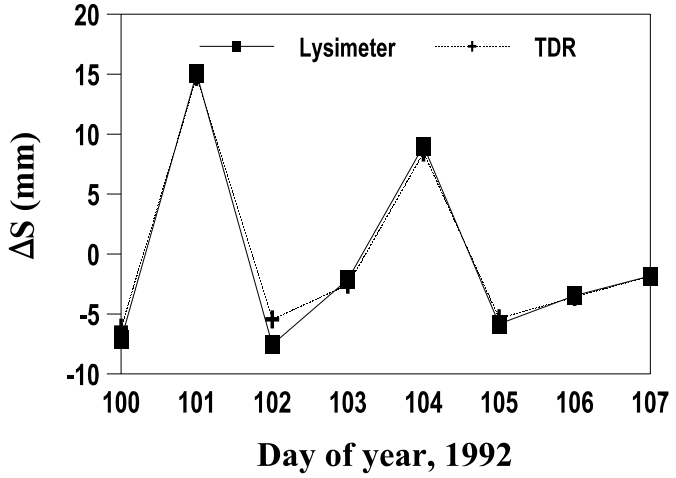

Fig. 5.36. Daily change in storage for the 35-cm and 2.4-m profiles from Fig. 5.35

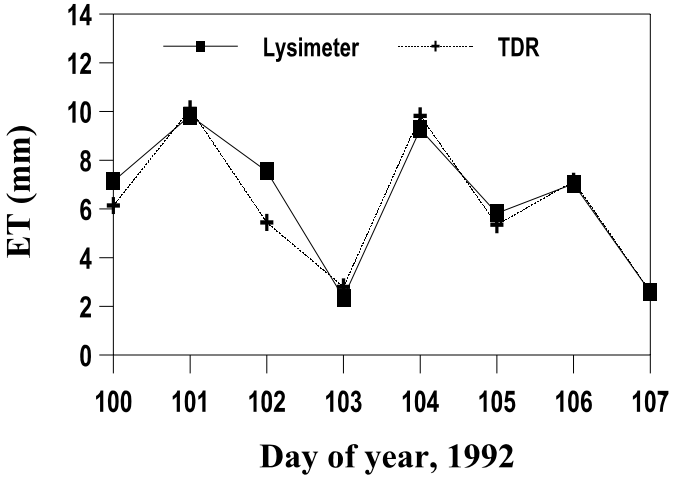

Fig. 5.37. Daily evapotranspiration as calculated from the TDR and weighing lysimeter data shown in Figs. 5.35 and 5.36

Example 5.7: Neutron Scattering – Sword to Plowshare.

At the end of World War II, the understanding of nuclear physics had increased tremendously, in particular the interactions of neutrons with atoms, which knowledge was essential to the development of the atomic bomb and fission reactors. There was a concerted effort to turn this knowledge to productive and peaceful uses, most of it funded by the US government. In 1950, the Civil Aeronautics Administration published Technical Report 127, describing a method for measuring soil moisture based on neutron scattering (Belcher et al., 1950). Independently, Wilford Gardner and Don Kirkham developed essentially the same method, which was published in Soil Science (Gardner and Kirkham, 1952). Oddly, the invention was probably aided by a lack of technology - specifically the difficulty of building a detector of fast (~5 million electron volts, MeV) neutrons, and the relative ease of building an efficient detector of thermal neutrons (~0.025 eV). Early detectors were often based on 3He, which has a large cross-section for the (n,p) interaction (Table 5B.2) in which an alpha particle (+1 charge) is ejected and detected electronically. The method is based on two facts, i) of the elements common in soils, hydrogen is by far the most effective in converting fast neutrons to thermal neutrons through collisions, and ii) of the hydrogen bearing soil constituents, water is usually the most plentiful and the only one that changes rapidly to an important extent. The slowing of neutrons by a particular atomic nucleus is affected both by the mass number, A, of the nucleus and the nuclear cross section, σ_a. For all scattering angles, Gardner and Kirkham gave the mean ratio, ε', of the energy of the neutron after a collision to its energy before as

$$\varepsilon' = 1 - \frac{A-1}{2A}\log_e \frac{A+1}{A-1}$$

Using this equation, calculate values of ε' for the elements in Table 5B.2. Note that the nuclear cross section for interaction with a neutron varies in size depending on the speed of the neutron. The larger the cross section, the larger the probability that a neutron will interact with an atom.

It would be difficult to overestimate the importance of the neutron scattering method in soil science and hydrological research and development over the last fifty years. It was the first useful, nondestructive method of repeatedly sampling the moisture content of soil profiles throughout and below the root zone. It led to the widespread measurement of crop water use values that are essential to irrigation management and the planning of large scale irrigation developments. After fifty years, a panel of scientists, expert in soil water measurement using time domain reflectometry (TDR), capacitance, and neutron scattering methods, convened by the International Atomic Energy Agency, recommended that the neutron scattering method not be replaced in the agency's research and training programs (IAEA, 2000). Three reasons were given: i) the method measures a relatively large volume of soil compared with TDR and capacitance instruments and so integrates across small-scale variability of soil properties and reduces the number of measurements needed, as well as reducing the sensitivity of the method to soil disturbance caused by installation, ii) the method is reliable and easy to use compared with others, and iii) the technology is mature, which brings to bear a large knowledge base of proven solutions to particular problems of use. To this I would add that the large volume of measurement makes field calibration much easier than it is for TDR and capacitance probes.

Problem 5.4. Neutron Facts of Life.

Given this information, discuss why the neutron scattering method is sensitive to the hydrogen content of soil, but relatively insensitive to other common elements. Discuss why application of large amounts of nitrogenous fertilizer might interfere with neutron probe measurements. Also, discuss why soils with large amounts of chloride salts would require different calibrations for water content vs. count of slow neutrons; and, discuss why the use of polyvinylchloride (PVC) plastic for access tubing causes the precision of neutron probe calibrations to decline relative to the precision obtained with aluminum or steel tubing (Dickey et al., 1993).

Table 5B.2. Values of atomic mass number, A, energy loss ratio, ε', and neutron scattering cross section, σ_a (1 barn = 10^{-24} cm^2). Adapted from Gardner and Kirkham (1952).

Element	A	ε'	σ_a (barns) Fast neutrons 5 MeV	σ_a (barns) Thermal neutrons 0.025 eV
H	1		2.55	47.5
^{3}He	3		2 (0.37)†	4 (5400)
C	12		1.60	4.6
N	14		1.0	18.0
O	16		1.5	4.2
Cl	17		2.7	40.0
Na	23		2.6	3.6
Mg	24		2.0	3.5
Al	27		2.5	1.6
Si	28		3.2	2.5
P	31		3.0	4.0
S	32		2.6	1.3
K	39		3.8	3.0
Ca	40		4.9	1.5
Mn	55		3.0	12.0
Fe	56		13.0	3.0

†Data for ^{3}He are from the Evaluated Nuclear Data Files W3 Retrieval System of Brookhaven National Laboratory, Upton, NY 11973-5000 (http://www.nndc.bnl.gov/nndc/endf/ Verified 15 May 2000). Numbers in parentheses are for the (n,p) interaction in which a neutron is captured and an alpha particle ejected. This is the reaction used in ^{3}He neutron detector tubes.

Water balance measurement intervals commonly range between hours and weeks and are usually no smaller than the required period of LE measurement. Measurement of each variable in Equation [5.81] presents its own unique problems. These include measurement errors in determination of lysimeter mass or ΔS, and errors in P and R measurement. Problems of P and R measurement are essentially identical for either weighing lysimetry or soil profile water content methods, because the surface area of the control volume can be defined for both methods with a water-tight border, often consisting of a sheet metal square or rectangle pressed into or partially buried in the soil surface. When the soil volume is unbounded below the surface, as in the soil profile water content method, there are additional errors due to uncontrolled horizontal flow components and deep percolation that are difficult to measure or estimate. Nevertheless, the profile water balance technique is applicable in many situations for which lysimetry is inappropriate or impossible and is, in addition, much less expensive. In many cases the horizontal flow components may be assumed to sum to zero; and deep percolation may be nil if the soil profile water content measurements are made to sufficient depth (Wright, 1990).

When neutron scattering alone is used to measure soil water content, the soil water balance method is suitable for periods of several days or more if closure ($F = 0$) at the bottom of the measured soil profile can be obtained (Wright, 1990). Neutron scattering (NS) is the most common water content measurement technique used (Cuenca, 1988; Wright, 1990) but due to the small changes in water content associated with daily ET and the limited precision of NS near the soil surface this water balance method has usually been restricted to measurement of ET over several day periods (Carrijo and Cuenca, 1992). Evett et al. (1993) showed that time domain reflectometery (TDR) measurements of soil water content near the surface could be coupled with deeper water content measurements by NS to close the water balance considerably more precisely than NS alone, opening up the prospect for daily ET measurements by this method.

5.3.2 Estimating Flux Across the Lower Boundary

One of the great advantages of lysimeters is that they control the soil water flux, F, into and out of the control volume. To date, a reliable soil water flux meter has not been developed, so F must be estimated if it is not controlled. If water flux across the lower boundary of the control volume is vertical it may sometimes be estimated by measurements (preferably multiple) of soil water potential, h, at different depths separated by distance, Δz, and knowledge of the dependence of hydraulic conductivity, K (m s^{-1}), on soil water potential - the K(h) curve. The potential difference, Δh, coupled with the unit hydraulic gradient for vertical flux, gives the hydraulic head difference, ΔH, driving soil water flux. Averaging the measurements allows estimation of the mean hydraulic conductivity for the soil layer between the measurements from the K(h) curve, and thus estimation of the soil water flux, J_w (m s^{-1}), from a finite difference form of Darcy's law

$$J_w = -K\left(\frac{\Delta H}{\Delta z}\right) \qquad [5.83]$$

Soil water potential may be measured by tensiometer or other means described in Section A, Chapter 3 (or see van Genuchten et al., 1991). Methods of measuring or estimating the K(h) curve may be found in Section A, Chapter 4. For fluxes across boundaries too deep for the installation of tensiometers the soil water content may be measured at two or more depths by neutron scattering (see Chapter 3) and the soil water potential inferred by inverting the $\theta(h)$ relationship, which may be estimated or measured (see Chapter 3 or van Genuchten et al., 1991). Due to the hysteresis of the $\theta(h)$ relationship there is more room for error when baseing J_w estimates on θ measurements. But, for many cases, the soil water potential will be in the range where hysteresis is not a large source of error (drier soils), and hydraulic conductivity is not large either. Thus, both the value of J_w and the error in J_w may be small enough for practical use.

Example 5.8: Deep Flux Loss or Gain in Soil Water Balance Calculation.

Figure 5B.4 shows the profile water content measured for a Pullman clay loam. Assume that the parameters in van Genuchten's equation (Equation [3.31]) are $\theta_s = 0.424$ m^3 m^{-3}, $\theta_r = 0.01$ m^3 m^{-3}, $\alpha = 0.88$ m^{-1}, n = 1.15, and m = 1 - 1/n. For the 2.10 and 2.30-m depths, use the water contents shown and calculate ψ_m for each depth by inverting Equation [3.31]. Use the same parameter values and water contents in Mualem's equation (Equation [4.62]) and calculate the hydraulic conductivities at each depth. Use Equation [5.83] to calculate the flux between the depths (use the mean hydraulic conductivity). If these conditions persisted for a week during which evaporation averaged 10 mm d^{-1}, what would be the absolute error in water content calculated using Equation [5.81] and ignoring flux across the lower boundary? What would the error be as a percentage of the weekly total E? Assume that measurements were taken to only 1.5 m and repeat the calculations using water contents from the 1.3 and 1.5-m depths. What are the errors in E (absolute and percentage), and are the errors larger or smaller? Why? How accurate do you think our calculations of F are? When using the water balance method for E of furrow-irrigated alfalfa, Wright (1990) measured to 3-m depth with the neutron probe; yet he found that flux across the lower boundary or water extraction by plant roots deeper than 3 m caused E estimates to be lower than those from a weighing lysimeter. For sprinkler-irrigated alfalfa, he found that water balance and lysimeter measurements agreed. Why did this happen?

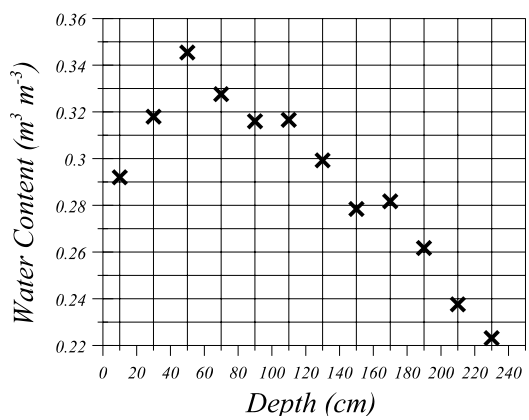

Fig. 5B.4. Soil water content of a Pullman soil measured by neutron scattering in an alfalfa field.

5.3.3 Precipitation and Runoff

An in-depth discussion of precipitation and runoff measurement and modeling is beyond the scope of this chapter. A classic and still valuable reference on field hydrologic measurements is the Field Manual for Research in Agricultural Hydrology (Brakensiek et al., 1979). A more up to date and extensive reference is the ASCE Hydrology Handbook, 2nd Edition (ASCE, 1996). Flow measurement in channels is detailed in Flow Measuring and Regulating Flumes (Bos et al., 1983). The monograph Hydrologic Modeling of Small

Fig. 5.38 H-flume and recorder (in white box) for measuring runoff rate from a graded bench terrace at Bushland, TX. Note dike diverting flow from uphill flume

Watersheds (Haan et al., 1982) included useful chapters on stochastic modeling, precipitation and snowmelt modeling, runoff modeling, etc.; and listed some 75 hydrologic models available at that time. For soil water balance measurements, runoff is often controlled with plot borders or edging driven into the ground or included as the above ground extension of a lysimeter. Steel borders driven into the soil to a depth of 20 cm will suffice in many situations. Sixteen gauge galvanized steel in rolls 30 cm wide is useful for this, and can be reinforced by rolling over one edge. If runoff must be measured this can be done with flumes such as the H-flume and recording station shown in Fig. 5.38.

Precipitation varies so much from location to location that it is rarely useful to attempt estimating it. Measurement methods include standard U.S. Weather Bureau rain gauges read manually, various tipping bucket rain gauges, heated gauges to capture snow fall (e.g Qualimetrics model 6021, Sacramento, CA), snow depth stations, etc. If possible, a rain gauge should be surrounded by a wind shield to avoid catch loss associated with wind flow over the gauge (Fig. 5.39). A standard for the capture area or throat of a rain gauge is that it should be 20 cm in diameter because smaller throats lead to more variability in amount captured. Various designs of tipping bucket rain gauge have become standard equipment on field weather stations. These are capable of providing precipitation data needed to solve the soil water balance for short intervals. Two problems are sometimes associated with tipping bucket type gauges. First, most of these devices count the tips using a Hall effect sensor for detecting the magnetic field of a magnet attached to the tipping bucket; and the sensing system is sometimes susceptible to interference from sources of electromagnetic noise such as vehicle ignition systems. Second, tipping bucket gauges do not keep up with very high rainfall rates. At Bushland, Texas we have observed tipping bucket errors of 10-15% for totals of rainfall from high intensity convective thunderstorms compared with amounts collected in standard rain gauges and sensed by weighing lysimeters. If accuracy is very important then a tipping bucket gauge should be supplemented with a standard gauge that captures and stores all the rainfall. For solving the soil water balance, experience shows that the rain gauge(s) should be placed directly adjacent to the location of ΔS measurement. Separation of even 100 m can lead to large errors due to the spatial variability of precipitation.

For studies and operations at scales larger than small plot size there are now precipitation estimates from Doppler radar based systems that offer calibrated rainfall data on a 24 h basis (Fig. 5.40) (see also Legates et al., 1996; and Vieux and Farajalla, 1996). Although Fig. 5.40 shows large grid sizes and only 16 levels

Fig. 5.39 Wind shield installed around a heated, tipping bucket rain gauge

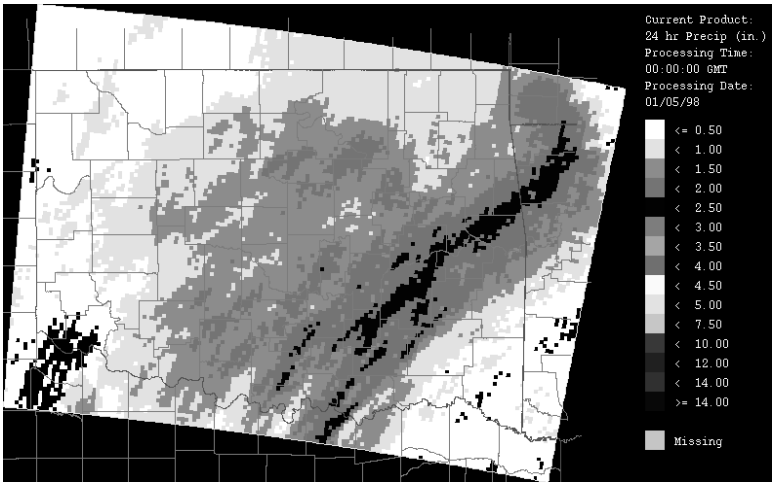

Fig. 5.40 Map of 24-h rainfall accumulation over Oklahoma. From NEXRAD radar data processed by the RPI. Image downloaded from http://ccgwww.ou.edu/rip_images and converted to gray scale. With permission

of precipitation; grid sizes of 4 km on a side, with 256 levels of rainfall, are available. Data for these maps are generated by the WSR-88D radar system, usually known as the NEXRAD weather radar system, in widespread use in the U.S. The Center for Computational Geosciences at the University of Oklahoma has developed a radar-base precipitation interface (RPI) for the radar data to generate the maps. Radar data are used from two or more stations and calibrated against rain gauge measurements available from, for example, the Oklahoma MESONET system of weather stations.

Acknowledgements

Much of the data presented in this chapter was collected by the Evapotranspiration Research Team at the USDA-ARS Conservation & Production Research Laboratory at Bushland, Texas, of which the author is a member. Other past and present team members are (alphabetically) Karen S. Copeland, Donald A. Dusek, Terry A. Howell, Arland D. Schneider, Jean L. Steiner, Rick W. Todd, and Judy A. Tolk. Many technicians supported the data collection efforts including C. Keith Brock, Jim L. Cresap, and Brice B. Ruthardt, among many others. Some of the data shown here have not yet been published and may appear at a later date in a peer reviewed journal. This work was supported in part by USAID under the subproject title Water Requirements and Management for Maize under Drip and Sprinkler Irrigation, a part of the Agricultural Technology Utilization and Transfer Project, Egypt. "Everything can be taken from a person except the freedom to choose one's attitude in any situtation" - a favorite quote of Ruby O. Crosby.

5.4 REFERENCES

Aase, J.K., and S.B. Idso. 1975. Solar radiation interactions with mixed prairie rangeland in natural and denuded conditions. Arch. Met. Geoph. Biokl. Ser. B, 23, 255-264.

Allen, R.G., M. Smith, A. Perrier, and L.S. Pereira. 1994a. An update for the definition of reference evapotranspiration. ICID Bulletin 43(2):1-34.

Allen, R.G., M. Smith, A. Perrier, and L.S. Pereira. 1994b. An update for the calculation of reference evapotranspiration. ICID Bulletin 43(2):35-92.

Alsanabani, M.M. 1991. Soil Water Determination by Time Domain Reflectometry: Sampling Domain and Geometry. Ph.D. thesis. Department of Soil and Water Sciences, Univ. of Arizona, Tucson. 209 pp.

Anlauf, R., K. Ch. Kersebaum, L.Y. Ping, A. Nuske-Schüler, J. Richter, G. Springob, K.M. Syring, and J. Utermann. 1990. Models for Processes in the Soil - Programs and Exercises. Catena Verlag, Cremlingen, West Germany.

ASAE. 1988. Modeling Agricultural, Forest, and Rangeland Hydrology: Proceedings of the 1988 International Symposium, Dec. 12-13, Chicago, IL. 1988. Amer. Soc. Agric. Eng., St. Joseph, MI.

ASCE. 1996. Hydrology Handbook, 2nd ed. Amer. Soc. Civil. Eng., New York, NY

Asrar, G., and E.T. Kanemasu. 1983. Estimating thermal diffusivity near the soil surface using Laplace Transform: uniform initial conditions. Soil Sci. Soc. Am. J. 47:397-401.

Baker, J.M., and R.J. Lascano. 1989. The Spatial Sensitivity of Time-Domain Reflectometry. Soil Sci. 147:378-384.

Baker, J.M., and E.J.A. Spaans. 1994. Measuring water exchange between soil and atmosphere with TDR-microlysimetry. Soil Sci. 158(1):22-30.

Ben-Asher, J., A.D. Matthias, and A.W. Warrick. 1983. Assessment of evaporation from bare soil by infrared thermometry. Soil Sci. Soc. Am. J. 47:185-191.

Black, T.A., G.W. Thurtell, and C.B. Tanner. 1968. Hydraulic load cell lysimeter, construction, calibration, and tests. Soil Sci. Soc. Am. Proc. 32:623-629.

Blad, B.L., and N.J. Rosenberg. 1974. Lysimetric calibration of the Bowen ratio energy balance method for evapotranspiration estimation in the central Great Plains. J. Appl. Meteorol. 13:227-236.

Bos, M.G., J.A. Replogle, and A.J. Clemmens. 1983. Flow Measuring and Regulating Flumes. I.L.R.I., Wageningen, The Netherlands, and U.S. Water Conservation Laboratory, Phoeniz, AZ.

Bowers, S.A., and R.J. Hanks. 1965. Reflection of radiant energy from soils. Soil Sci. 100(2):130-138.

Brakensiek, D.L., H.B. Osborn, and W.J. Rawls. 1979. Field Manual for Research in Agricultural Hydrology. U.S. Dept. Agric., Agricultural Handbook 224. U.S. Govn. Printing Office.

Brunt, D. 1932. Notes on radiation in the atmosphere. Quart. J. Roy. Met. Soc. 58:389-418.

Brutsaert, W. 1975. The roughness length for water vapor, sensible heat and other scalars. J. Atm. Sci. 32:2028-2031.

Brutsaert, W. 1982. Evaporation Into The Atmosphere. D. Reidel Pub. Co., Boston, MA.

Campbell, G.S. 1977. An Introduction to Environmental Biophysics. Springer-Verlag, New York.

Campbell, G.S. 1985. Soil Physics with BASIC - Transport Models for Soil-Plant Systems. Elsevier, New York.

Campbell, G.S., C. Calissendorff, and J.H. Williams. 1991. Probe for measuring soil specific heat using a heat-pulse method. Soil Sci. Soc. Am. J. 55:291-293.

Campbell, G.S., J.D. Jungbauer, Jr., W.R. Bidlake, and R.D. Hungerford. 1994. Predicting the effect of temperature on soil thermal conductivity. Soil Sci. 158(5):307-313.

Carrijo, O.A., and R.H. Cuenca. 1992. Precision of evapotranspiration measurements using neutron probe. J. Irrig. and Drain. Engrg. ASCE, 118(6):943-953.

Chen, J. 1984. Mathematical analysis and simulation of crop micrometeorology. Ph.D. Diss. Agricultural Univ. Wageningen, The Netherlands.

Cochran, P.H., L. Boersma, and C.T. Youngberg. 1967. Thermal conductivity of a pumice soil. Soil Sci. Soc. Am. Proc. 31:454-459.

Collares-Pereira, M., and A. Rabl. 1979. The average distribution of solar radiation - Correlations between diffuse and hemispherical and between daily and hourly insolation values. Solar Energy 22:155-164.

Costello, T.A., and H.J. Braud, Jr. 1989. Thermal Diffusivity of Soil by Nonlinear Regression Analysis of Soil Temperature Data. Trans. ASAE 32(4):1281-1286.

Cuenca, R.H. 1988. Model for evaptranspiration using neutron probe data. J. Irrig. and Drain. Engrg., ASCE, 114(4):644-663.

De Vries, D.A. 1963. Chapter 7. Thermal properties of soils. *In* W.R. Van Wijk (ed.) Physics of Plant Environment. North-Holland Publ. Amsterdam.

Doorenbos, J., and W.O. Pruitt. 1977. Guidelines for predicting crop water requirements. FAO Irrigation and Drainage Paper 24. Food and Agriculture Organization of the United Nations, Rome.

Duffie, J.A., and W.A. Beckman. 1991. Solar Engineering of Thermal Processes, 2nd Ed. John Wiley & Sons, New York.

Dugas, W.A., and W.L. Bland. 1991. Springtime soil temperatures in lysimeters in Central Texas. Soil Sci. 152(2):87-91.

Dugas, W.A., L.J. Fritchen, L.W. Gay, A.A. Held, A.D. Matthias, D.C. Reicosky, P. Steduto, and J.L. Steiner. 1991. Bowen ratio, eddy correlation, and portable chamber measurements of sensible and latent heat flux over irrigated spring wheat. Agric. Forest Meteorol. 56:1-20.

Dvoracek, M.J., and B. Hannabas. 1990. Prediction of albedo for use in evapotranspiration and irrigation scheduling. *In* Visions of the future, proceedings of the third national irrigation symposium held in conjunction with the 11th annual international irrigation exposition. Oct. 28-Nov. 1, Phoenix, AZ. ASAE, 2950 Niles Rd., St. Joseph, MI 49085-9659, USA.

Evett, S.R. 1994. TDR-Temperature arrays for analysis of field soil thermal properties. Pp. 320-327 *In* Proceedings of the Symposium on Time Domain Reflectometry in Environmental, Infrastructure and Mining Applications, Sept. 7-9, 1994. Northwestern University, Evanston, Illinois.

Evett, S.R., T.A. Howell, J.L. Steiner, and J.L. Cresap. 1993. Evapotranspiration by soil water balance using TDR and neutron scattering. Pp. 914-921 *In* R.G. Allen and C.M.U. Neale (eds.) Management of Irrigation and Drainage Systems, Integrated Perspectives. Am. Soc. Civil Engr., New York, NY. Proceedings of the National Conference on Irrigation and Drainage Engineering, Park City, UT, July 21-23, 1993.

Evett, S.R., and R.J. Lascano. 1993. ENWATBAL: A mechanistic evapotranspiration model written in compiled BASIC. Agron. J. 85:763-772.

Evett, S.R., A.D. Matthias, and A.W. Warrick. 1994. Energy balance model of spatially variable evaporation from bare soil. Soil Sci. Soc. Amer. J. 58:1604-1611.

Evett, S.R., A.W. Warrick, and A.D. Matthias. 1995. Wall material and capping effects on microlysimeter performance. Soil Sci. Soc. Amer. J. 59:329-336.

Fox, M.J. 1968. A technique to determine evaporation from dry stream beds. J. Appl. Meteorol. 7:697-701.

Gates, D.M. 1980. Biophysical Ecology. Sprinker-Verlag, New York.

Gorry, P.A. 1990. General least-squares smoothing and differentiation by the convolution (Savitsky-Golay) method. Anal. Chem. 62:570-573.

Goudriaan, J. 1977. Crop micrometeorology: A simulation study. PUDOC, Wageningen, The Netherlands.

Grebet, R., and R.H. Cuenca. 1991. History of lysimeter design and effects of environmental disturbances. Pp 10-19 In Lysimeters for Evapotranspiration and Environmental Measurements, Proceedings of the International Symposium on Lysimetry, July 23-25, 1991, Honolulu, Hawaii. ASCE 345 E. 47th St., NY, NY 10017-2398.

Hanks, J., and J.T. Ritchie (eds.). 1991. Modeling Plant and Soil Systems. Agronomy Monograph 31. Amer. Soc. Agron., Crop Sci. Soc. Amer., Soil Sci. Soc. Amer., Madison, WI.

Hann, C.T., H.P. Johnson, and D.L. Brakensiek (eds.). 1982. Hydrologic Modeling of Small Watersheds. ASAE Monograph No. 5. Amer. Soc. Agric. Eng., 2950 Niles Road, St. Joseph, MI.

Hatfield, J.L., R.J. Reginato, and S.B. Idso. 1983. Comparison of long-wave radiation calculation methods over the United States. Water Resour. Res. 19:285-288.

Heilman, J.L., C.L. Brittin, and C.M.U. Neale. 1989. Fetch requirements for Bowen ratio measurements of latent and sensible heat fluxes. Agric. and Forest Meteorol. 44:261-273.

Hillel, D. 1980. Fundamentals of Soil Physics. Academic Press, San Diego.

Horton, R., P.J. Wierenga, and D.R. Nielsen. 1983. Evaluation of methods for determining the apparent thermal diffusivity of soil near the surface. Soil Sci. Soc. Am. J. 47:25-32.

Houser, P.R. 1998. Personal communication from Paul R. Houser, Hydrological Sciences Branch, Data Assimilation Office, NASA Goddard Space Flight Center.

Houser, P.R., C. Harlow, W.J. Shuttleworth, T.O. Keefer, W.E. Emmerich, and D.C. Goodrich. 1998. Evaluation of multiple flux measurement techniques using water balance information at a semi-arid site. *In* Proc. Special Symp. on Hydrology, Amer. Meteorol. Soc. Conf., Phoenix, AZ, pp. 84-87.

Howell, T.A., A.D. Schneider, D.A. Dusek, T.H. Marek, and J.L. Steiner. 1995. Calibration and scale performance of Bushland weighing lysimeters. Trans. ASAE 38(4):1019-1024

Howell, T.A., A.D. Schneider, and M.E. Jensen. 1991. History of lysimeter design and use for evapotranspiration measurements. Pp 1-9 In Lysimeters for Evapotranspiration and Environmental Measurements, Proceedings of the International Symposium on Lysimetry, July 23-25, 1991, Honolulu, Hawaii. ASCE 345 E. 47th St., NY, NY 10017-2398.

Howell, T.A., J.L. Steiner, S.R. Evett, A.D. Schneider, K.S. Copeland, D.A. Dusek, and A. Tunick. 1993. Radiation balance and soil water evaporation of bare Pullman clay loam soil. Pp. 922-929 *In* R.G. Allen and C.M.U. Neale (eds.) Management of Irrigation and Drainage Systems, Integrated Perspectives. Am. Soc. Civil Engr., New York, NY. Proceedings of the National Conference on Irrigation and Drainage Engineering, Park City, UT, July 21-23, 1993.

Howell, T.A., J.L. Steiner, A.D. Schneider, S.R. Evett, and J.A. Tolk. 1994. Evapotranspiration of irrigated winter wheat, sorghum and corn. ASAE paper no. 94-2081, 33 pp.

Howell, T.A., and J.A. Tolk. 1990. Calibration of soil heat flux transducers. Theor. Appl. Climatol. 42:263-272.

Idso, S.B. 1981. A set of equations for full spectrum and 8- to 14-μm and 10.5- to 12.5 μm thermal radiation from cloudless skies. Water Resour. Res. 17(2)295-304.

Idso, S.B., and R.J. Reginato. 1974. Assessing soil-water status via albedo measurement. Hydrol. Water Resour. Ariz. Southwest 4:41-54.

Idso, S.B., R.D. Jackson, R.J. Reginato, B.A. Kimball, and F.S. Nakayama. 1975. The dependence of bare soil albedo on soil water content. J. Appl. Meteorol. 14(1)109-113.

Idso, S.B., R.J. Reginato, R.D. Jackson, B.A. Kimball, and F.S. Nakayama. 1974. The three stages of drying in a field soil. Soil Sci. Soc. Amer. Proc. 38(5),831-837.

Iwata, S., T. Tabuchi, and B.P. Warkentin. 1988. Soil-Water Interactions: Mechanisms and Applications. Marcel Dekker, Inc., New York.

Jensen, M.E., R.D. Burman, and R.G. Allen (ed). 1990. Evapotranspiration and Irrigation Water Requirements. ASCE Manuals and Reports on Engineering Practices No. 70, ASCE, New York. 332 pp.

Jones, H.G. 1992. Plants and Microclimate: A Quantitative Approach to Environmental Plant Physiology. 2nd Ed. The Cambridge University Press, Cambridge, UK.

Kimball, B.A., R.D. Jackson, R.J. Reginato, F.S. Nakayama, and S.B. Idso. 1976. Comparison of field measured and calculated soil heat fluxes. Soil Sci. Soc. Am. J. 40:18-24.

Kluitenberg, G.J., K.L. Bristow, and B.S. Das. 1995. Error analysis of heat pulse method for measuring soil heat capacity, diffusivity, and conductivity. Soil Sci. Soc. Am. J. 59:719-726.

Kondo, J., N. Saigusa, and T. Sato. 1992. A model and experimental study of evaporation from bare-soil surfaces. J. Applied Meteor. 31:304-312.

Kreith, F., and W.D. Sellers. 1975. General principles of natural evaporation. p. 207-227. *In* D.A. de Vries and N.H. Afgan (ed.) Heat and Mass Transfer in the Biosphere. Part 1. John Wiley & Sons, New York

Lascano, R.J., C.H.M. van Bavel, J.L. Hatfield, and D.R. Upchurch. 1987. Energy and water balance of a sparse crop: simulated and measured soil and crop evaporation. Soil Sci. Soc. Am. J. 51:1113-1121.

Lascano, R.J., and J.L. Hatfield. 1992. Spatial variability of evaporation along two transects of a bare soil. Soil Sci. Soc. Am. J. 56:341-346.

Legates, D.R., K.R. Nixon, T.D. Stockdale, and G. Quelch. 1996. Soil water management using a water resource decision support system and calibrated WSR-88D precipitation estimates. Proc. AWRA Symp. GIS and Water Resources. Amer. Water Resources Assoc., Fort Lauderdale, FL.

List, R.J. 1971. Smithsonian Meteorological Tables. Smithsonian Institution Press, Washington.

Lourence, F., and R. Moore. 1991. Prefabricated weighing lysimeter for remote research stations, Pp. 423-439 *In* Lysimeters for Evapotranspiration and Environmental Measurements, Proceedings of the International Symposium on Lysimetry, July 23-25, 1991, Honolulu, Hawaii. ASCE 345 E. 47th St., NY, NY 10017-2398.

Marek, T.H., A.D. Schneider, T.A. Howell, and L.L. Ebeling. 1988. Design and construction of large weighing monolithic lysimeters. Trans. ASAE 31:477-484.

McCullough, E.C., and W.P. Porter. 1971. Computing clear day solar radiation spectra for the terrestrial ecological environment. Ecology 52:1008-1015.

Moncrieff, J.B., J.M. Massheder, H.A.R. De Bruin, J. Elbers, T. Friborg, B. Heusinkveld, P. Kabat, S. Scott, H. Soegaard, and A. Verhoef. 1997. A system to measure surface fluxes of momentum, sensible heat, water vapour and carbon dioxide. J. Hydrol. 189:589-611.

Monteith, J.L. 1961. The reflection of short-wave radiation by vegetation. Q.J. Roy. Meteorol. Soc. 85(366):386-392.

Monteith, J.L. 1965. Evaporation and the environment. In The State and Movement of Water in Living Organisms. XIXth Symp. Soc. for Exp. Biol., Swansea, Cambridge University Press. pp. 205-234.

Monteith, J.L., and G. Szeicz. 1961. The radiation balance of bare soil and vegetation. Q.J. Roy. Meteorol. Soc. S7 (372):159-170.

Monteith, J.L., and M.H. Unsworth. 1990. Principles of Environmental Physics, 2nd Ed. Edward Arnold, London.

Murray, F.W. 1967. On the computation of saturation vapor pressure. J. Applied Meteorol. 6(1):203-204.

Nassar. I.N., and R. Horton. 1989. Determination of The Apparent Thermal Diffusivity of a Nonuniform Soil. Soil Sci. 147(4):238-244.

Nassar, I.N., and R. Horton. 1990. Determination of Soil Apparent Thermal Diffusivity from Multiharmonic Temperature Analysis for Nonuniform Soils. Soil Sci. 149(3):125-130.

NOAA. 1997. Data files UARS96.PLT, ERBS.PLT, NOAA09.PLT, NOAA10.PLT, NIMBUS.PLT, and SMM.PLT. Accessed January 14, 1998.
From ftp://ftp.ngdc.noaa.gov/STP/SOLAR_DATA/SOLAR_IRRADIANCE/.

Noborio, K., K.J. McInnes, and J.L. Heilman. 1996. Measurements of soil water content, heat capacity, and thermal conductivity with a single TDR probe. Soil Sci. 161(1):22-28.

Oke, T.R. 1978. Boundary Layer Climates, Methuen, New York.

Peart, R.M., and R.B. Curry. 1998. Agricultural Systems Modeling and Simulation. Marcel Dekker, Inc., New York.

Penman, H.L. 1948. Natural evapotranspiration from open water, bare soil and grass. Proc. R. Soc. London Ser. A. 193:120-145.

Pereira, L.S., B.J. van den Broek, P. Kabat, and R.G. Allen (eds.). 1995. Crop-Water-Simulation Models in Practice. Wageningen Pers, Wageningen, The Netherlands.

Richter, J. 1987. The Soil as a Reactor: Modeling Processes in the Soil. Catena Verlag, Cremlingen, West Germany.

Riha, S.J., K.J. McKinnes, S.W. Childs, and G.S. Campbell. 1980. A finite element calculation for determining thermal conductivity. Soil Sci. Soc. Am. J. 44:1323-1325.

Ritchie, J.T., T.A. Howell, W.S. Meyer, and J.L. Wright. 1996. Sources of biased errors in evaluating evapotranspiration equations. Pp. 147-157 *In* C.R. Camp, E.J. Sadler, and R.E. Yoder (eds.) Evapotranspiration and Irrigation Scheduling, Proceedings of the International Conference. Nov. 3-6, 1996, San Antonio, TX.

Rosenberg, N.J. 1969. Seasonal patterns of evapotranspiration by irrigated alfalfa in the Central Great Plains. Agron. J. 61(6):879-886.

Rosenberg, N.J., B.L. Blad, and S.B. Verma. 1983. Microclimate, the biological environment. John Wiley & Sons, New York.

Russell, G., B. Marshall, and P.G. Jarvis (eds). 1989. Plant Canopies: Their Growth, Form and Function. Cambridge University Press, Cambridge UK.

Savage, M.J., K.J. McInnes, and J.L. Heilman. 1995. Placement height of eddy correlation sensors above a short turfgrass surface. Agric. Forest Meteor. 74(3-4):195-204.

Savage, M.J., K.J. McInnes, and J.L. Heilman. 1996. The "footprints" of eddy correlation sensible heat flux density, and other micrometeorological measurements. South African Journal of Science 92:137-142.

Savitsky, A., and M.J.E. Golay. 1964. Smoothing and differentiation of data by simplified least squares. Anal. Chem. 36:1627-1639.

Schmid, H.P. 1997. Experimental design for flux measurements: matching scales of observations and fluxes. Agric. Forest Meteorol. 87:179-200.

Schneider, A.D. 1998a. Personal communication. Drawing of cross-section of simplified weighing lysimeter installed at Bushland, TX.

Schneider, A.D. 1998b. Personal communication. Drawing of cross-section of large weighing lysimeter at Bushland, TX.

Schneider, A.D., T.A. Howell, T.A. Moustafa, S.R. Evett, and W.S. Abou-Zeid. 1996. A simplified weighing lysimeter for developing countries. Pp. 289-294 *In* C.R. Camp, E.J. Sadler, and R.E. Yoder (eds.) Proceedings of the International Conference on Evapotranspiration and Irrigation Scheduling. Nov. 3-6, 1996, San Antonio, Texas, U.S.A. 1166 pp.

Schuepp, P.J., M.Y. LeClerc, J.I. MacPherson, and R.L. Desjardins. 1990. Footprint prediction of scalar fluxes from analytical solutions of the diffusion equation. Boundary-Layer Meteorol. 50:355-373.

Sepaskhah, A.R., and L. Boersma. 1979. Thermal conductivity of soils as a function of temperature and water content. Soil Sci. Soc. Am. J. 43: 439-444.

Skidmore, E.L., J.D. Dickerson, and H. Schimmelpfennig. 1975. Evaluating surface-soil water content by measuring reflection. Soil Sci. Soc. Am. J. 39:238-242.

Spitters, C.J.T., H.A.J.M. Toussaint, and J. Goudriaan. 1986. Separating the diffuse and direct component of global radiation and its implications for modeling canopy photosynthesis. Part I. Components of incoming radiation. Agric. Forest Meteorol. 38:217-229.

Todd, R.M. 1998a. Personal communication, analysis of footprint of Bowen ratio system over alfalfa field at Bushland, Texas.

Todd, R.M. 1998b. Personal communication, Bowen ratio results for period between 3rd and 4th cuttings of alfalfa at Bushland, Texas in 1997.

Unland, H.E., P.R. Houser, W.J. Shuttleworth, and Z-L. Zang. 1996. Surface flux measurement and modeling at a semi-arid Sonoran desert site. Agric. Forest Meteorol. 82:119-153.

van Bavel, C.H.M. 1966. Potential evaporation: The combination concept and its experimental verification. Water Resour. Res. 2:455-467.

van Bavel, C.H.M., and D.I. Hillel. 1976. Calculating potential and actual evaporation from a bare soil surface by simulation of concurrent flow of water and heat. Agric. Meteorol. 17:453-476.

van Genuchten, M. Th., F.J. Leij, and S.R. Yates. 1991. The RETC code for quantifying the hydraulic functions of unsaturated soils. EPA/600/2-91/065. 93 pp. R.S. Kerr Environ. Res. Lab., U.S. Environmental Protection Agency, ADA, OK.

Van Wijk, W.R., and D.W. Scholte Ubing. 1963. Radiation. p. 62-101. In W.R. Van Wijk (ed.), Physics of plant environment. North-Holland Pub. Co., Amsterdam.

Verma, S.B., N.J. Rosenberg, and B.L. Blad. 1978. Turbulent exchange coefficients for sensible heat and water vapor under advective conditions. J. Appl. Meteorol. 17:330-338.

Vieux, B.E., and N.S. Farajalla. 1996. Temporal and spatial aggregation of NEXRAD rainfall estimates on distributed storm runoff simulation. Third Intl. Conf. GIS and Environmental Modeling, Jan. 21-25, 1996, Santa Fe, NM.

Watts, D.B., E.T. Kanemasu, and C.B. Tanner. 1990. Modified heat-meter method for determining soil heat flux. Agric. Forest Meteor. 49:311-330.

Weast, R.C. (ed). 1982. Handbook of Chemistry and Physics. CRC Press.

Weiss, A. 1982. An experimental study of net radiation, its components and prediction. Agron. J. 74:871-874.

Wierenga, P.J., D.R. Nielson, and R.J. Hagan. 1969. Thermal properties of a soil, based upon field and laboratory measurements. Soil Sci. Soc. Am. J. 44: 354-360.

Wraith, J.M., and J.M. Baker. 1991. High-resolution measurement of root water uptake using automated time-domain reflectometry. Soil Sci. Soc. Am. J. 55:928-932.

Wright, J.L. 1982. New evapotranspiration crop coefficients. J. Irrig. and Drain. Div. ASCE. 108(IR1):57-74.

Wright, J.L. 1990. Comparison of ET measured with neutron moisture meters and weighing lysimeters. Pp. 202-209 in Irrigation and Drainage: Proceedings of the National Conference. Durango, Colorado, July 11-13, 1990. ASCE, New York.

Wright, J.L. 1991. Using weighing lysimeters to develop evapotranspiration crop coefficients. *In* R.G. Allen, T.A. Howell, W.O. Pruitt, I.A. Walter, and M.E. Jensen (ed.) Lysimeters for Evapotranspiration and Environmental Measurements. Proceedings of the International Symposium on Lysimetry, July 23-25, Honolulu, Hawaii. ASCE, New York.

Wright, J.L., and M.E. Jensen. 1972. Peak water requirements of crops in Southern Idaho. J. Irrig. and Drain. Div. ASCE 96(IR1):193-201.

Young, M.H., P.J. Wierenga, and C.F. Mancino. 1997. Monitoring near-surface soil water storage in turfgrass using time domain reflectometry and weighing lysimetry. Soil Sci. Soc. Am. J. 61:1138-1146.